الجمـــهوريـــة الجـــزائريـــة الديـمقـراطيـــــــة الشـــعبيـــــة
PEOPLE'S DEMOCRATIC REPUBLIC OF ALGERIA
وزارة التعليم العالي والبحث العلمي
MINISTRY OF HIGHER EDUCATION AND SCIENTIFIC RESEARCH
جامعة عمّار ثليجي بالأغواط
AMAR TELIDJI UNIVERSITY OF LAGHOUAT
كلية العلوم
FACULTY OF SCIENCES
Materials Science DEPARTMENT

Master's dissertation

Domain: *Materials science*
Field: *Physics*
Option: *Materials physics*

*By M^me^* ***SAILAA Namarek.***

On the subject:

Ab-initio study of the structural, electronic, optical, and mechanical properties of the ternary compounds *ABSe3 (A = Cs, Tl).*

Publicly discussed on July 06th, 2022 in front of the jury composed of:

Mr. LEFKAIER Ibn Khaldoun	Professor	President
Mr. ARAR Rabie	Doctor	Examiner
Mr. MAABED Said	Doctor	Examiner
Mr. HALIT Mohammed	Professor	Supervisor
Mr. KHEMLOUL Fakhereddine	PhD Student	Co-supervisor

University year 2021-2022

When you change the way you look at things,

the things you look at change.

Dedication

I am dedicating my dissertation to beloved people who have meant and continue to mean so much to me.

To my family and many friends.

First and foremost, my mother Wahiba "Mama" who raised me, loved me, and whose words of encouragement and push for tenacity ring in my ears.
Next, to my father Belkhier whose love for me knew no bounds and, who taught me the value of hard work. Thank you so much "Abii",

A special feeling of gratitude for my loving sister Nafissa, who has always loved me unconditionally and whose good examples have taught me to work hard for the things that I aspire to achieve. My brothers Mohammed and Moufdi have never left my side and are very special and cute.

I also dedicate this to my husband, Omer, who has been a constant source of support and encouragement during the challenges of graduate school and life. I am truly thankful for having you in my life.

*My wonderful daughter **Ilaf**, the miniature version of me who made this work harder and more challenging and gave it a flavor of value.*

I love you all beyond words.

Last but not least I am dedicating this to my true friends who have supported me throughout the process. I will always appreciate all they have done,
I dedicate this work and give special thanks to my best friends Aroua. and Rokaya for being there for me throughout the entire master's program. Both of you have been my best cheerleaders.

تمارق

Acknowledgments

الحمد لله الذي هدانا لهذا وماكنا لنهتدي لولا ان هدانا الله.

First of all, I would like to warmly thank the University of Amar Telidji of Laghouat.

It is very difficult for me to express my gratitude and appreciation to my supervisor **Pr. HALIT Mohammed** and co-supervisor **PhD. KHEMLLOUL Fakhereddine**, I know how hard it is to be struggling with health issues I wish you both soon recovery...

I wish to thank my committee members who were more than generous with their expertise and precious time. A special thanks to ***Pr. LEFKAIER Ibn Khaldoun,*** my committee chairman for his countless hours of reflecting, reading, advising, and most of all patience throughout the entire process.

Dr. ARAR Rabie and ***Dr. MAABED Said,*** for agreeing to serve on my committee. I am privileged to have you as my examiners now I know my work is in good hands to be as best as possible, Thanks a million times.

Special thanks go to ***Mrs. Dr. HAMDI Rokaya*** who inspired hope, ignite my imagination, and stood for me when I needed.

Pr. HELIFA Bachir was a compass that activates the magnets of curiosity, knowledge, and wisdom in us, he instills a love of learning in me. Endless thanks and appreciation for his continued support.

One of the most important things we can do to show our gratitude, is to make sure that we say thank you when someone helps us out, to ***PhD. EL DJEMAI Ataellah*** I owe you a debt of gratitude for your support, I appreciate your willingness to share your experiences with me, your reward is in haven, to *Pr. FAYED Fares, PhD. BELLI Ayoub, PhD. BOULEBDA Hicham, Dr. FADLA Abdelillah.*

Finally, I would like to acknowledge and thank all the teachers, and administrators in our department division. Their excitement and willingness to provide feedback made the completion of this research an enjoyable experience.

Table of Contents

List of Abbreviations:

CASTEP: Cambridge Serial Total Energy Package.

DFPT: density functional perturbation theory.

DOS: Density of states.

GGA: Generalized Gradient Approximation.

GGA-PBE: Generalized Gradient Approximation Perdew-Burk-Ernzerhof.

LDA: Local Density Approximation.

PDOS: Partial density of states.

TDOS: Total density of states.

PP: Pseudo-potential.

PW: Plane Wave.

SCF: Self Consistent Field.

US-PP: Ultrasoft pseudopotential.

BZ : Brillouin zone.

$ABSe_3$: *A = Cs, Tl.*

List of Figures

List of Tables

→ *"Not only is the Universe stranger than we think, it is stranger than we can think."*

GENERAL INTRODUCTION . . .

INTRODUCTION

In order to exploit materials in the industry, it is necessary to ensure their quality by checking on some physical and chemical properties. Materials science is an increasingly important field that applies in several technological applications, and in many areas that would help ensure novel materials quality [1].

Lately a new and unexplored area of research is appeared called the selenoborates.

The difficult chemistry of boron-sulfur and boron-selenium compounds covers a vast array of structural motifs [2]. The chemistry of boron is recognized to be peculiar in all of its forms. Additionally, it exhibits a strong propensity to produce amorphous products across a broad temperature range. Both characteristics combine in the compounds with the heavier chalcogens, sulfur, and selenium to open a fascinating field to the preparative chemist, crystallographer, physicist, and theorist. Modern preparative techniques produced innovative and frequently surprising boron-sulfur and boron-selenium compounds some 40 years ago [3].

Only a dozen alkali metal and monovalent thallium boron-selenide compounds have been structurally characterized by single-crystal X-ray analysis [4]. One of the most challenging and exciting problems in materials research and development is predicting the crystal structure of materials from fundamental principles. Density functional theory (*DFT*) has been shown to be one of the most accurate methods for calculating the physical properties of solids, so we have different approaches to understanding them: empirical, semi-empirical, and first-principles approaches. These first principles are known as the ab initio majority in functional density theory, which states that knowledge of the electron density can determine the properties of the ground state. Several calculation methods have been developed over the last few decades, in particular ab-initio methods which have now become an essential tool in calculating the physical properties of the most complex systems. They are also a tool of choice for predicting new materials and they have sometimes been able to replace very expensive experiments [5].

To extract the different physical and chemical properties of molecular systems, the laws of quantum mechanics are applied. In the 1920s, Erwin Schrödinger (*1933 Nobel Prize in Physics*) [6] gave a mathematical formalization of the motion of a set of electrons and atoms in the form of the wave equation. This equation is the cornerstone of quantum mechanics. Unfortunately, it is only utterly soluble in atomic or molecular systems consisting of only one electron. For systems with a large number of electrons, we must settle approximations. Therefore, the aim is to obtain a

solution from the Schrödinger equation that is as close as possible to the solution of the real system [7].

The calculations presented in this manuscript were carried out using two numerical modeling codes, one called *CASTEP* and the other called *CRYSTAL09*.

CASTEP can predict physical properties including elastic constants, structural properties, energy band diagrams, electronic densities of states, charge densities, and optical properties as well as vibrational and thermodynamic properties [8]. While the code *CRYSTAL09* makes it possible to calculate the energy of the ground electronic state, the energy gradient, the electronic wave function, and the electronic structure of periodic systems by the Hartree-Fock or DFT approach with the possibility of using various functionals [9].

This study aims to determine the structural, electronic, optical, and elastic properties of $CsBSe_3$ and $TlBSe_3$ compounds, which revealed a wide variety of physical properties, making it a candidate material for many applications in optoelectronics, geophysics, catalysis, and the environment [10].

The compounds of $ABSe_3$ where $(A = Cs, Tl)$ caught our interest since we assumed they must be difficult because they belong to a unique family of materials (*THE PERSELENOBORATES*).

The investigation of the structural, electrical, elastic, and optical characteristics of $ABSe_3$ compounds is the focus of this brief dissertation.

• *The dissertation is organized into three main axes:*

The first chapter gives some general informations on the physical properties of the compounds $ABSe_3$.

In the second chapter, we represent the theory on which are based our calculations of structural, electronic, and elastic properties…. namely the Density Functional Theory (*DFT*) as well as the elastic properties of a material.

The third chapter is devoted to the results and discussions obtained by our calculations.

First, we present the crystal structure of the studied materials and the calculation details. Then, we present our results and their interpretations relating to the structural, electronic, elastic and optical properties of the compounds $ABSe_3$.

Finally, we end our thesis with a general conclusion.

References

[1]. Smith, W. F. (1986). Principles of materials science and engineering.

[2]. Conrad, O., Jansen, C., & Krebs, B. (1998). Bor-Schwefel-und Bor-Selen-Verbindungen–von Prinzipien einzigartiger Molekülstrukturen zu neuartigen Polymermaterialien. *Angewandte Chemie*, *110*(23), 3396-3407.

[3]. *Angew. Chem. Int. Ed.* **1998**, Conrad. Boron Sulfur and Boron Selenium Compounds From Unique Molecular Structural Principles.

[4]. a) O. Conrad, C. Jansen, B. Krebs, *Angew. Chem.***110**3396(1998); *Angew. Chem. Int. Ed.* **37** 3208 (1998); b) O. Conrad, B. Krebs, *Phosphorus, Sulfur, and Silicon* **124/125** 37 (1997).

[5]. Qian, G., González-Albuixech, V. F., Niffenegger, M., & Giner, E. (2016). Comparison of KI calculation methods. *Engineering Fracture Mechanics*, *156*, 52-67.

[6]. Danylova, T. V., & Komisarenko, S. V. (2020). Nobel prize winner Erwin Schrödinger: the physicist, philosopher, and godfather of molecular biology and genetics. *Ukr Biochem J*, *92*(3), 93-100.

[7]. Feit, M. D., Fleck Jr, J. A., & Steiger, A. (1982). Solution of the Schrödinger equation by a spectral method. *Journal of Computational Physics*, *47*(3), 412-433.

[8]. Segall, M., et al., *First-principles simulation: ideas, illustrations and the CASTEP code.* Journal of Physics: Condensed Matter, 2002. 14(11): p. 2717.

[9]. R. Dovesi, A. Erba, R. Orlando, C.M. Zicovich-Wilson, B. Civalleri, L. Maschio, M. Rerat, S. Casassa, J. Baima, B. Salustro, B. Kirtman, CRYSTAL17 User's Manual, (2017).

[10]. Lindemann, A., Küper, J., Hamann, W., Kuchinke, J., Köster, C., & Krebs, B. (2001). Syntheses, crystal structures, and properties of the three novel perselenoborates RbBSe3, CsBSe3, and TlBSe3 with polymeric chain anions. *Journal of Solid State Chemistry*, *157*(1), 206-212.

→ *"I don't know anything, but I do know that everything is interesting if you go into it deeply enough."*

– Richard Feynman –

CHAPTER -I-

State Of Art

In this chapter an overview of the Perselenoborates who are a large class of solid compounds, they are usually described by the chemical formula ABQ_3 where A can be alkali metal, post-transition metal, etc., B is the element Boron and (Q = Se: Selenium, S: Sulfur).

They can be prepared from metal selenides, amorphous boron, and selenium.

I-1. Introduction

In recent years, significant advances in synthetic techniques have enabled the synthesis and characterization of a large number of thioborates and selenoborates [1, 2]. The crystal structures of compounds known today consist of several unique types of chalcogenide borate anions, which coordinate with different metal cations. The observed structural principles suggest that boron is in three different chalcogen coordination.

Binary boron sulfides and selenides [1, 3-5], as well as various thioborates and selenoborates, contain anions in which trigonal plane-coordinated boron occurs. Small isolated units with high negative charge, such as BS_3^{3-} [6-8], BSe_3^{3-} [9], $B_2S_4^{2-}$ [10], $B_2S_5^{2-}$ [11], or $B_3S_6^{3-}$ [8, 12-14] are characteristic structural motifs of non-oxide chalcogenide borates of alkali and alkaline earth metals or monovalent thallium.

For boron in tetrahedra surrounded by sulfur or selenium, the BQ_4 monomers occurs more condensed *(Q = Se, S)*, but the isolated BS_4^{5-} anions are so far unknown. The smallest oligomers are tetrameric $B_4S_{10}^{8-}$ units [15,16]; various polymer chains [17,18], layers [19,20], and network structures [21-23] result from the condensation of BQ_4 units. Recently, a new structural feature was observed in boron chalcogenide chemistry: the discovery of new $[B_{12}(BSe_3)_6]^{8-}$ anions in the ternary and quaternary compounds $A_8[B_{12}(BSe_3)_6]$ and $Hg_2A_4[B_{12}(BSe_3)_6]$ (A = *Rb, Cs*) [24,25]. These anions are assembled from compact clusters of six BSe_3 units fully saturated with selenium.

I-1-1. Selenoborates

It is well known that boron-containing compounds have interesting chemical and physical properties, moreover, boron shows a high tendency to form amorphous products over a wide temperature range. In compounds with heavier chalcogens, sulfur and selenium, these two features combine to open up an interesting field.

The study of non-oxide boron chalcogenides is hampered by severe experimental difficulties, one of which is the inherent tendency to vitrify. This class of compounds rejected their study due to various problems [2]:

- Difficult to obtain high-purity elemental boron.

- Material selection for reaction vessels has been difficult for many years, because quartz glass is attacked by boron at high temperatures (*B/Si* mass exchange through the formation of B_2O_3 and SiQ_2 ($Q = S, Se$)), and chalcophiles Most metals do not include the usual metal containers.

- The reaction products and often even the starting materials are susceptible to oxidation and/or hydrolysis by air and moisture.

- Chalcogenoborates tend to remain amorphous rather than crystalline.

I-2. The synthesis of $CsBSe_3$ & $TlBSe_3$

$CsBSe_3$ can be prepared from the metal selenides, amorphous boron, and selenium, while in the case of $TlBSe_3$ directly from the elements.

Solid-state reactions were carried out in carbon-coated silica tubes under a vacuum at high temperatures.

Both substances $CsBSe_3$ & $TlBSe_3$ comprise polymeric anionic chains with the formula $([BSe_3]^-)_n$, which are made up of nonplanar, five-membered B_2Se_3 rings that have been Spiro cyclically fused and have boron atoms in a tetrahedral BSe_4 coordination. The novel compounds' vibrational spectra were measured, and X-ray powder patterns are described [26].

Through experimentation, the following steps were taken to synthesize each of these materials:

I-2-1. $CsBSe_3$

Within 4 hours, a mixture of Cs_2Se, amorphous boron, and selenium in a 1: 2: 5 molar ratio was heated to $970\ ^\circ K$ and maintained at this temperature for 2 hours.

The sample was cooled to $870\ ^\circ K$ for 10 hours, then *to* $670\ ^\circ K$ for another 24 hours before being annealed for crystallization and then linearly cooled to $470\ ^\circ K$ in 120 hours.

Quantitative yields of deep-red plate-shaped crystals were achieved. On coming into touch with a preparation needle, the crystals split into tiny needles with a parallel alignment [26].

I-2-2. *$TlBSe_3$*

Elemental thallium, amorphous boron, and selenium were present in the sample in the molar ratios of 1:1:2.9. The sample was heated to *950 °K* in just 8 hours and held there for 4 hours.

The sample was annealed for crystallization with linear cooling to *520 °K* within 120 h after chilling during 16 h to *820 °K*.

The yield was quantitative and included deep-red needles. On contact with a preparation needle, the crystals once more explode into very fine, long, parallel needles of opposite orientation.

All goods were handled in a glove box under dry argon because they are all sensitive to air and moisture [26]**.**

I-3. Examination of crystal structure

Crystal structures were ascertained using X-ray data from a single crystal. *$CsBSe_3$*, the alkali metal perselenoborate, crystallizes in the *$P2_1/c$* monoclinic space group, while *$TlBSe_3$*, the post-transition metal perselenoborate, crystallizes in the *Cc* monoclinic space group.

- ***Table I-1.*** provides information on the parameters as well as specifics on the solutions and structure-related improvements.

- ***Table I-2.*** displays the coordinates of every atom, average temperature factors, and their predicted norm deviations.

Table I-1.: Crystal data, measurement details and, structure solution of both compounds [26].

Empirical method	***$CsBSe_3$***	***$TlBSe_3$***
Formula weight [g/mol]	380.60	452.06
Color	deep red	deep red
Crystal system	Monoclinic	Monoclinic
Space group	$P2_1/c$ (no°. 14)	Cc (no°. 9)
Lattice constants	a= 7.570(2) Å b= 12.791(4) Å c = 6.171(2) Å β= 107.09(2) °	a= 6.166(2) Å b= 12.109(2) Å c = 7.031(2) Å β= 113.88(3) °
Cell volume ($Å^3$)	571.1(3)	480.1(2)
Formula units per cell	4	4
Calculated density (g/cm^3)	4.426	6.255
Crystal dimensions	0.10 x 0.09 x 0.05 mm^3	0.12 x 0.04 x 0.04 mm^3
Temperature (°K)	293(2)	213(2)
Diffractometer	SIEMENS P3	STOE IPDS
Radiation, wavelength	Mo *Kα*, (λ= 0.71073 Å)	Mo *Kα*, (λ= 0.71073 Å)
Range in hkl	$-9 \leq h \leq 9$ $-16 \leq k \leq 0$ $0 \leq l \leq 7$	$-7 \leq h \leq 7$ $-16 \leq k \leq 16$ $-9 \leq l \leq 9$
Absorption coefficient	25.4 mm^1	56.2 mm^1
Extinction coefficient	0,0018(2)	0,0007(4)

Table I-2.: Standard deviations for the isotropic displacement parameters (Å^2) and atomic coordinates [26].

Atom	*x*	*y*	*z*	U_{eq}[1]
		$CsBSe_3$		
Cs	0.26101(9)	0.42256(5)	0.21280(11)	0.0326(2)
B	0.7056(14)	0.2693(7)	0.1534(16)	0.0184(19)
Se (1)	0.93819(13)	0.18176(7)	0.16211(15)	0.0226(2)
Se (2)	0.79989(13)	0.40665(6)	0.31961(15)	0.0232(2)
Se (3)	0.54755(12)	0.19467(6)	0.33231(14)	0.0202(2)
		$TlBSe_3$		
Tl	0.76104(11)	0.67554(5)	0.78902(10)	0.0320(3)
B	0.329(3)	0.5239(11)	0.248(2)	0.013(3)
Se (1)	0.2472(3)	0.66737(12)	0.3608(3)	0.0208(4)
Se (2)	0.5305(2)	0.43361(16)	0.51192(18)	0.0178(4)
Se (3)	0.5127(3)	0.55269(12)	0.0693(2)	0.0179(3)

I-4. Structure Description

The $[(BSe_3)^-]_n$ chains in perselenoborates have a unique structural characteristic that is a modified version of the chain structures known as "*Zweiereinfachketten*" seen in silicate chemistry [27] and in substances like $K_2SnS_3 \cdot 2\,H_2O$ [28], $PbGeS_3$ [29], and Na_2GeS_3 [30].

The three isotypic compounds with the formula ABS_3 (A = *Cs, Tl*) [2, 18, 31] exist in thioborate chemistry and represent the same structure type as the one above. While the thallium

[1] Considered to be a third of the orthogonalized tensor's trace.

perselenoborate $TlBSe_3$ exhibits the same structural property but crystallizes in the acentric space group *Cc*, whereas the alkali metal selenoborates $CsBSe_3$ is isotypic to these similar thioborates (space group $P2_1/c$).

The polymeric chain anions of composition $[(B_2Q_7)^{2-}]_n$ [2, 17, 32] and $[(B_3Q_{10})^{2-}]_n$ [18, 31] (*Q = S, Se)* perchalcogenoborates, which alternate five-membered B_2Se_3 and six-membered B_2Se_4 rings in ratios of 1:1 and 2:1, respectively, share additional structural characteristics.

The novel perselenoborates $CsBSe_3$ and $TlBSe_3$ have coordinating metal cations and polymeric chain anions of general composition $[(BSe_3)^-]_n$ in their structures A^+ [26].
Corner-sharing and almost undistorted BSe_4 tetrahedra are used to create the infinite one-dimensional anionic networks, which are further connected by a single diselenide bridge.
Parts of two polymeric anions can be found in every unit cell. A 2_1-screw axis along the crystallographic plane is present for the two isotypic alkali metal perselenoborates.

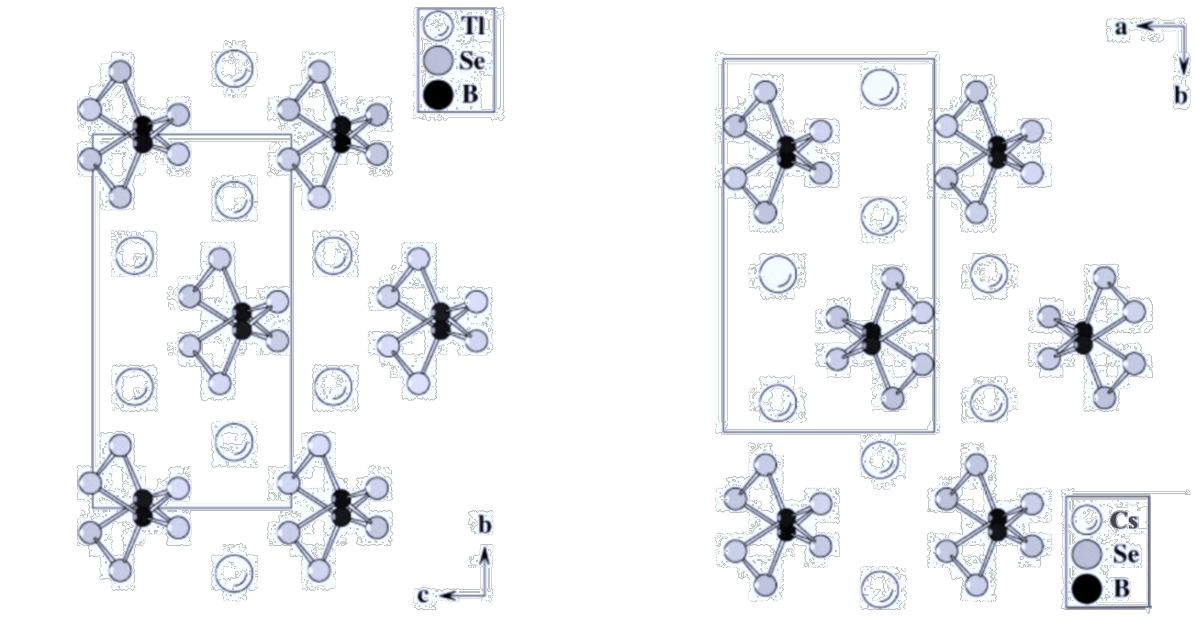

Fig I-1. Crystal structure of $TlBSe_3$ with parallel chains along [100] (*left*); Crystal structure of $CsBSe_3$ containing polymeric antiparallel chains along [001] (*right*) [26].

• The binary boron selenide $[(BSe_3)^-]_n$ is attacked by diselenide entities via nucleophilic attack, which is the formal building block of one-dimensional polymeric $[(BSe_2)]_n$-chain anions (*see* ***Fig I-2.***)

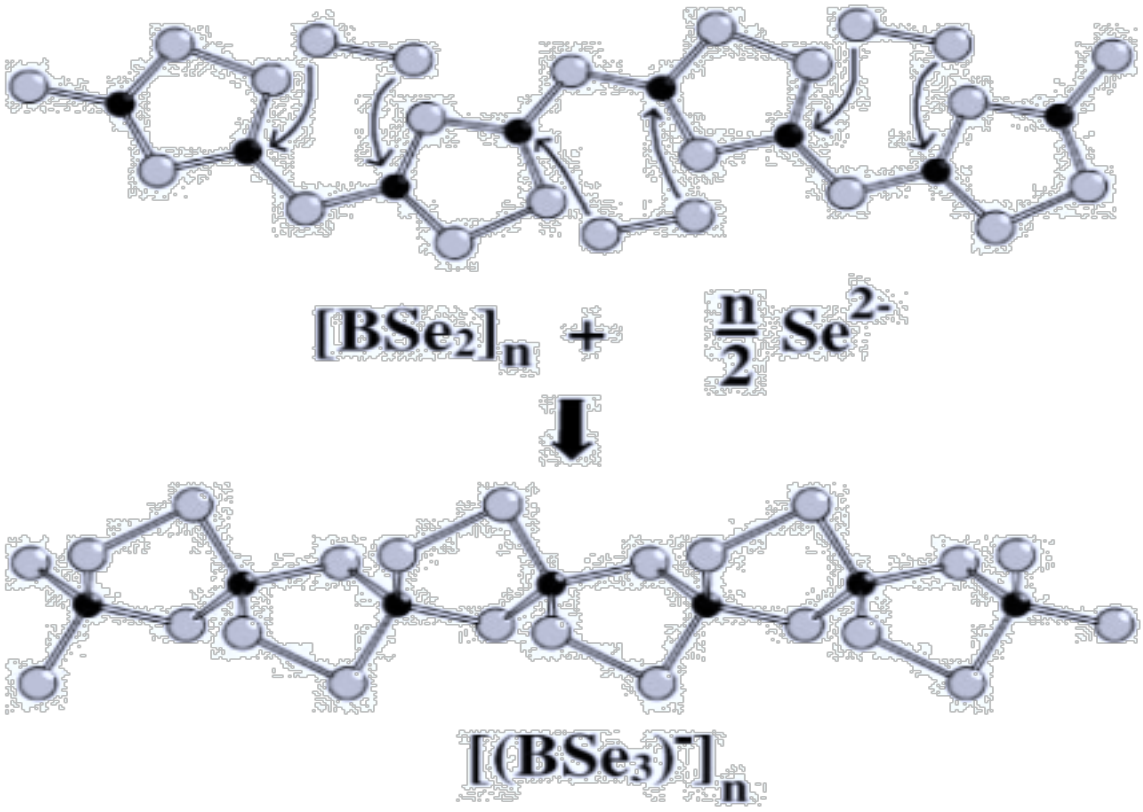

Fig I-2. Formal building mechanism [26].

• ***Fig I-2*** represent formal building mechanism of one-dimensional polymeric $[(BSe_3)^-]_n$-chain anions: nucleophilic attack of diselenide entities toward the binary boron selenide $[(BSe_2)]_n$.

I-5. The bonds

In each of our perselenoborates, the *Se—Se* distances are roughly equal. The average value of (2.355 Å) [26] is in excellent agreement with those in binary boron diselenide $[BSe_2]_n$ (2.347 Å) [2, 17, 32], whereas the perselenoborates containing B_2Se_2 rings show a slightly longer diselenide bridge (2.370 Å) [26].

All of the compounds average *Se—B—Se* angles total 109.4(5) ° [26], which is precisely the same as the ideal tetrahedral angle.

• ***Table I-3.*** lists the symmetry operations, selected bond lengths and angles, and bond lengths.

Ionic interactions link three chain anions to every cation. The *12* selenium atoms that make up the irregular ASe_{12} polyhedron that forms the coordination sphere of the alkali metal selenoborates.

If *Tl---Se* distances up to 4 Å are taken into account, the thallium cations are only *10-fold* coordinated by selenium in the case of $TlBSe_3$ [26].

Table I-3.: Selected Bond Lengths (Å) and Angles (°) in the Structures of CsBSe3, and $TlBSe_3$ with Standard Deviations [26].

$CsBSe_3$			
B—Se(1)	*2.074(10)*	Se(1)—B— Se(3c)	*113.4(4)*
B—Se(2)	*2.053(9)*	Se(2)—B— Se(3)	*107.3(4)*
B—Se(3)	*2.083(9)*	Se(2)—B—Se(3c)	*108.1(4)*
B—Se(3c)	*2.044(10)*	Se(3)—B—Se(3c)	*110.7(5)*
Se(1)—Se(2c)	*2.3541(14)*	B—Se(1)—Se(2c)	*94.9(3)*
Se(1)—B—Se(2)	*106.3(4)*	B—Se(2)—Se(1g)	*92.0(3)*
Se(1)—B—Se(3)	*110.7(4)*	B—Se(3)—B(1g)	*98.4(4)*
$TlBSe_3$			
B—Se(1)	*2.055(15)*	Se(1)—B— Se(3a)	*107.2(7)*
B—Se(2)	*2.076(14)*	Se(2)—B— Se(3)	*111.4(7)*
B—Se(3)	*2.034(17)*	Se(2)—B—Se(3a)	*112.5(7)*
B—Se(3a)	*2.065(14)*	Se(3)—B—Se(3a)	*109.0(7)*
Se(1)—Se(2a)	*2.358(3)*	B—Se(1)—Se(2a)	*90.5(4)*
Se(1)—B—Se(2)	*104.6(6)*	B—Se(2)—Se(1b)	*96.5(5)*
Se(1)—B—Se(3)	*112.2(7)*	B—Se(3)—B(1b)	*99.9(6)*

Description

The alkali metal perselenoborate $CsBSe_3$ is determined to have an average B—Se bond length of 2.064 Å. This bond distance is somewhat shorter in $TlBSe_3$ 2.058 Å, which can be attributed to the *low-temperature* measurement (*the difference is scarcely beyond the margin of error*). Both compounds have much higher average bond lengths than perselenoborates of the aforementioned compositions, which are perselenoborates of $Na_2B_2Se_7$, 2.044 Å [17]; $K_2B_2Se_7$, 2.050 Å [17]; $Rb_2B_2Se_7$, 2.049 Å [2, 32]; $Cs_3B_3Se_{10}$, 2.050 Å [2, 31].

Bond lengths in selenioborates with trigonal-planar-coordinated boron show considerable differences when compared. The later ones, which coordinate the B_{12} cluster in the compounds, $A_8[B_{12}(BSe_3)_6]$ and $Hg_2A_4[B_{12}(BSe_3)_6]$ (A = *Cs, Tl*) [24, 25] vary from 1.90 Å (in $[BSe_2]_n$) to 2.02 Å in the BSe_3 ligands.

I-6. Structure crystallography

•$TlBSe_3$ material crystallize in the monoclinic structure of the perselenoborate family with space group *Cc* (*ranked 9 in the international table of crystallography*) as shown in figure ***Fig I-4.***

•$CsBSe_3$ material crystallize in the monoclinic structure of the perselenoborate family as well with space group $P2_1/c$ (*ranked 14 in the international table of crystallography*) and the following figure shows that.

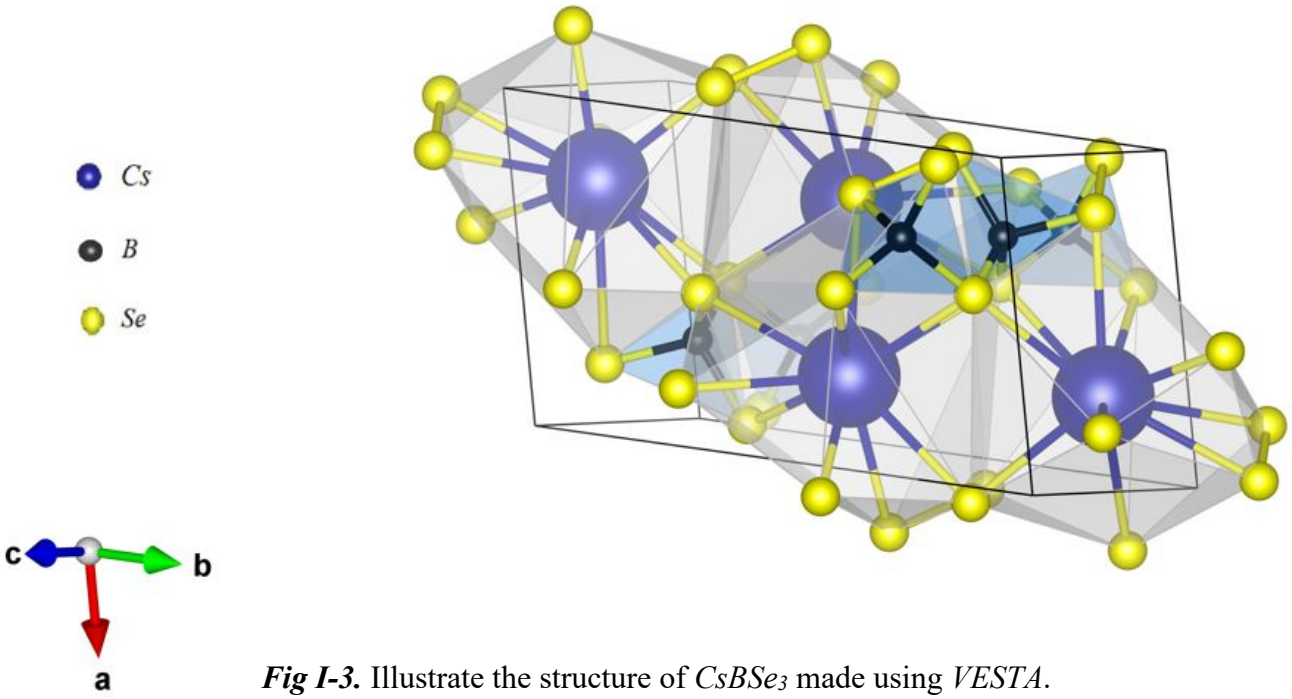

Fig I-3. Illustrate the structure of $CsBSe_3$ made using *VESTA*.

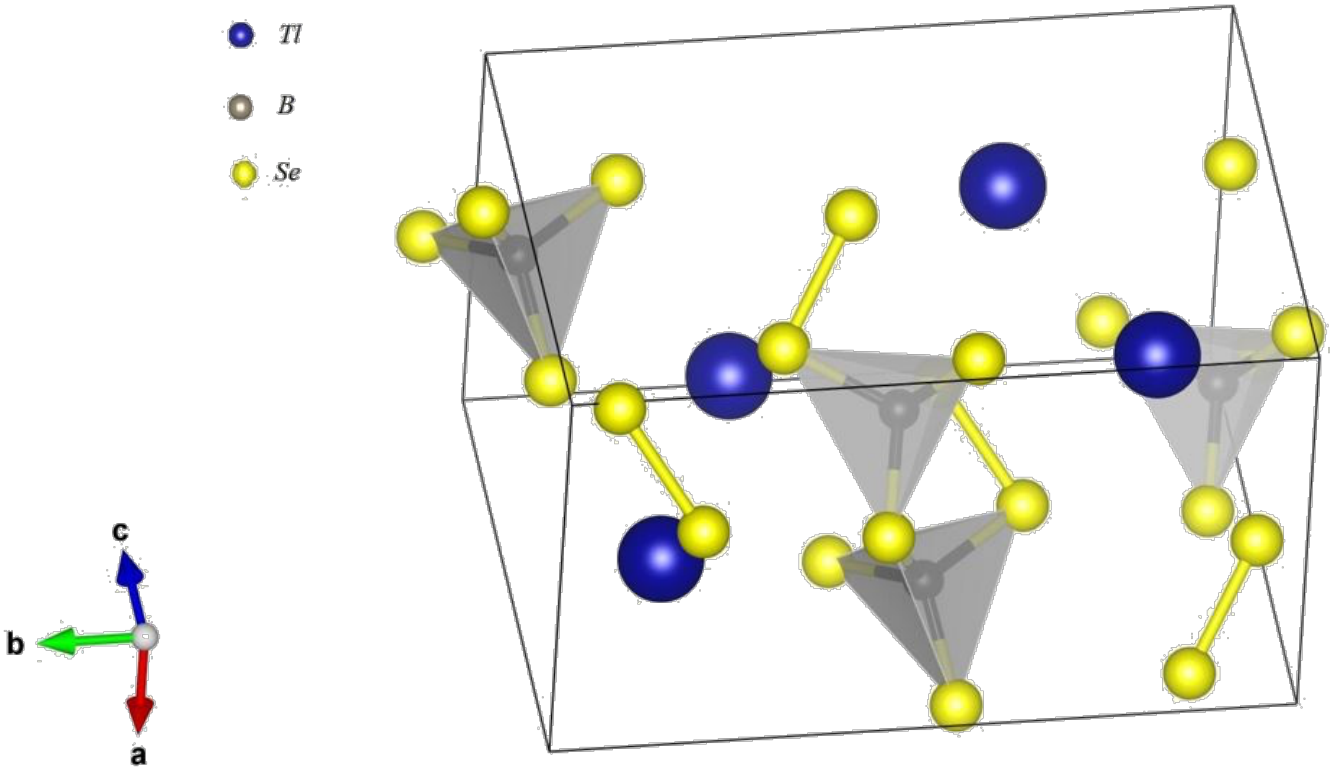

Fig I-4. Illustrate the structure of $TlBSe_3$ made using *VESTA*.

I. References

[1]. B. Krebs, *Angew. Chem.* **95,** 113 (1983); *Angew. Chem. Int. Ed. Engl.* **22,** 113 (1983).

[2]. O. Conrad, C. Jansen, and B. Krebs, *Angew. Chem.* **110,** 3396 (1998); *Angew. Chem. Int. Ed.* **37,** 3208 (1998).

[3]. P. zum Hebel, H. Diercks, and B. Krebs, *Z. Kristallogr.* **185,** 40 (1988).

[4]. B. Krebs and H.-U. Hürter, *Acta Crystallogr. Sect. A* **37,** C163 (1981).

[5]. B. Krebs and H.-U. Hurter, *Angew. Chem.* **92,** 479 (1980); *Angew. Chem. Int. Ed. Engl.* **19,** 481 (1980).

[6]. P. Vinatier, P. Gravereau, M. Menetrier, L. Trut, and A. Levasseur, *Acta Crystallogr. Sect. C* **50,** 1180 (1994).

[7]. F. Hiltmann, C. Jansen, and B. Krebs, *Z. Anorg. Allg. Chem.* **622,** 1508 (1996).

[8]. F. Hiltmann and B. Krebs, *Z. Anorg. Allg. Chem.* **621,** 424 (1995).

[9]. B. Krebs and W. Hamann, *J. ¸ess-Common Met.* **137,** 143 (1988).

[10]. A. Hammerschmidt, C. Jansen, J. Kuper, C. Puttmann, and B. Krebs, *Z. Anorg. Allg. Chem.* **621,** 1330 (1995).

[11]. C. Jansen, J. Kuper, and B. Krebs, *Z. Anorg. Allg. Chem.* **621,** 1322 (1995).

[12]. C. Püttmann, H. Diercks, and B. Krebs, *Phosphorus Sulfur Silicon* **65,** 1 (1992).

[13]. F. Chopin and A. Hardy, *C. R. Acad. Sci.* **261,** 142 (1965).
[14]. F. Chopin and G. Turrell, *J. Mol. Struct.* **3,** 57 (1969).

[15]. P. Hagenmuller, F. Chopin, and B. Castagna, *C. R. Acad. Sci. C* **262,** 418 (1966).

[16]. A. Hardy, *Bull. Soc. Fr. Mine&ral. Cristallogr.* **91,** 111 (1968).

[17]. A. Hammerschmidt, J. Kuper, L. Stork, and B. Krebs, *Z. Anorg. Allg. Chem.* **620,** 1898 (1994).

[18]. C. Puttmann, F. Hiltmann, W. Hamann, C. Brendel, and B. Krebs, *Z. Anorg. Allg. Chem.* **619,** 109 (1993).

[19]. F. Chopin and B. Capdepuy, *Bull. Soc. Chim. Fr.* 505 (1970).

[20]. C. Puttmann, W. Hamann, and B. Krebs, *Eur. J. Solid State Inorg. Chem.* **29,** 857 (1992).

[21]. P. zum Hebel, B. Krebs, M. Grune, and W. Muller-Warmuth, *Solid State Ionics* **43,** 133 (1990).

[22]. B. Krebs and H. Diercks, *Z. Anorg. Allg. Chem.* **518,** 101 (1984).

[23]. A. Hammerschmidt, P. zum Hebel, F. Hiltmann, and B. Krebs, *Z. Anorg. Allg. Chem.* **622,** 76 (1996).

[24]. J. Kuper, O. Conrad, and B. Krebs, *Angew. Chem.* **1997,** 109 (1995); *Angew. Chem. Int. Ed. Engl.* **36,** 1903 (1997).

[25]. A. Lindemann, J. Kuchinke, and B. Krebs, *Z. Anorg. Allg. Chem.* **625,** 1165 (1999).

[26]. Syntheses, Crystal Structures, and Properties of the Three Novel Perselenoborates *RbBSe3*, *CsBSe3*, and *TlBSe3* with Polymeric Chain Anions, Arno Lindemann, Journal of Solid-State Chemistry 157, 206_212 (2001).

[27]. F. Liebau, Naturwissenschaften 49, 41 (1962).

[28]. W. Schiwy, C. Blutau, D. GaK thje, and B. Krebs, Z. Anorg. Allg. Chem. 412, 1 (1975).

[29]. M. Ribes, J. Olivier-Fourcade, E. Philippot, and M. Maurin, Acta Crystallogr. Sect. B 30, 1391 (1974).

[30]. J. Olivier-Fourcade, E. Philippot, M. Ribes, and M. Maurin, Rev. Chim. Mine&r. 9, 757 (1972).

[31]. J. Küper, doctoral thesis, University of Münster (1996).

[32]. C. Jansen, doctoral thesis, University of Münster (1997).

→ *"The science of today is the technology of tomorrow.."*

– Edward Teller –

CHAPTER -II-

Theoretical Framework

We will follow the historical course of the development of these approximations in brief until the outcome of the DFT.

This is the subject of this chapter.

Where we will expose the different methods applied within the framework of the DFT to treat a solid environnement and how we can calculate the different physical properties of the solid using the DFPT (*density functional perturbation theory*).

II-1. Introduction

A solid is made up of a certain number of electrons in interaction under the effect of an external potential due to the nuclei or an external electric field, and which obey the laws of quantum mechanics. Electromagnetic interactions govern most of the observable properties of the solid, other forces are either short range or very weak in influencing the physical properties of solids. In the time-independent stationary case, one can access the properties of such a system by solving the appropriate Schrödinger equation. Such an equation is very complex (*many-body problem*), this is due to the long range of the Colombian interaction. So we have to make some approximations.

II-2. Schrödinger equation

"A differential equation which forms the basis of the quantum-mechanical description of matter in terms of the wave-like properties of particles in a field. Its solution is related to the probability density of a particle in space and time ".

Consider a solid body consisting of *N* nucleis and *e* electrons, the equation that describes this complex quantum system in its ground state is the time-independent[2] Schrödinger equation [1-4]:

$$H\psi = E\psi \qquad II-(01)$$

Where H is the Hamiltonian given by the following relation:

$$H = T_N + T_e + U_{N\_e} + U_{e\_e} + U_{N\_N} \qquad II-(02)$$

Such as:

T_N: Nuclei's kinetic energy.

T_e: Electrons kinetic energy.

[2] In order to simplify, spin and relativistic effects are not introduced.

U_{N_e}: Attractive nuclei-electron Coulomb interaction.

U_{e_e}: Repulsive electron-electron Coulomb interaction.

U_{N_N}: Coulomb repulsive nuclei-nuclei interaction.

E: Is the eigenvalue of the Hamiltonian, and represents the total energy of the system.

ψ: the system wave function which depends on the coordinates of the nucleus and electrons, $\psi: \psi[\{\boldsymbol{R}_i\}, \{\boldsymbol{r}_i\}]$.

With: $\{\boldsymbol{R}_i\} = \boldsymbol{R}_1, \boldsymbol{R}_2, \boldsymbol{R}_3, \ldots\ldots\ldots\ldots\ldots\ldots \boldsymbol{R}_N$ represents the set of nucleus coordinates.

$\{\boldsymbol{r}_i\} = \boldsymbol{r}_1, \boldsymbol{r}_2, \boldsymbol{r}_3, \ldots\ldots\ldots\ldots\ldots\ldots\ldots \boldsymbol{r}_N$ represents the set of electrons coordinates.

To facilitate calculations, it is more convenient to work with atomic units (a. u) than with *International System* (IS) units, these units are shown in the following table :

Table II.1: The atomic units used in DFT.

Sizes	*Symbol or expression in IS*	*Value in IS*	*Atomic unit (a. u)*
Electron mass	m_e	9.1094E-31 kg	1 a. u
Electron charge	$-e$	-1.6022E-19 C	1 a. u
Length (Bohr radius)	$a_0 = \frac{4\pi\varepsilon_0\hbar}{m_e e^2}$	5.2918E-11 m	1a. u = 1 Bohr
Strength	$F = \frac{E_0}{a_0}$	8.2387E-8 N	1 a. u = 1 Hartree/Bohr
Energy	$E_0 = \frac{\hbar^2}{m_e a_0^2}$	4.3597E-18 J	1 a. u = 1 Hartree
Action	$\hbar = \frac{h}{2\pi}$	1.0546E-34 J/s	1 a. u

II-3. The Born-Oppenheimer approximation

The first approximation made to solve equation II-(01) is the adiabatic approximation [5] made in 1926 by Born and Oppenheimer. It is based on the very large difference between the masses of nuclei and electrons (*it is less than E-5 for atoms heavier than calcium*). Therefore, the electronic relaxation is instantaneous with respect to the motion of the nuclei. Then we can write the wave function of the system as the product of two wave functions; one for the nuclei and the

other for the electrons which is the electronic wave function. Thus, the potential energy U_{N_N} becomes a constant[3]:

$$\psi[\{\boldsymbol{R}_i\},\{\boldsymbol{r}_i\}] = \psi_e[\{\boldsymbol{r}_i\};\{\boldsymbol{R}_i\}] \times \phi_N[\{\boldsymbol{R}_i\}] \qquad II-(03)$$

We are interested in the electronic wave function $\psi_e[\{\boldsymbol{r}_i\},\{\boldsymbol{R}_i\}]$ which should satisfy the equation:

$$H_e\psi_e = E_e\psi_e \qquad II-(04)$$

Where H_e is the electronic Hamiltonian given by:

$$H_e = T_e + U_{e\_e} + U_{N\_e} \qquad II-(05)$$

All the ab initio methods are based on these last two equations to calculate the electronic structure.

II-4. Hartree and Hartree-Fock approximation

A second approximation complements that of Born-Oppenheimer proposed by Hartree [6]. It is based on the free electron hypothesis, where the interactions between electrons and the spin states are not taken into account. Then the electronic wave function can be written as a mono electronic wave product:

$$\psi[\{\boldsymbol{r}_i\},\{\boldsymbol{R}_i\}] = \prod_{i=1}^{Ne} \psi_i\{\boldsymbol{r}_i\} \qquad II-(06)$$

And the system equations to be solved will be given by:

$$H_H\psi_i(\boldsymbol{r}_i) = \varepsilon_i\psi_i(\boldsymbol{r}_i) \qquad II-(07)$$

The general algorithm followed to solve these equations is said coherent auto or SCF (*Self Consists Field).*

The consequences of this approximate are:

- The total Colombian repulsion is overestimated.
- Pauli's principle is not respected.
- The exchange and correlation effects are not taken into account.

To correct all that, Hartree and Fock [7] proposed to express the multi-efficient wave function in the form of a determinant of Slater [8]:

[3] We can always introduce T_N and U_{N_N} to tackle the problem of lattice vibrations (phonons).

$$\psi_e = \psi_{SD} = \frac{1}{\sqrt{N!}} \begin{vmatrix} \psi_1(\boldsymbol{r}_1) & \psi_2(\boldsymbol{r}_1) & \cdots & \psi_N(\boldsymbol{r}_1) \\ \psi_1(\boldsymbol{r}_2) & \psi_2(\boldsymbol{r}_2) & \cdots & \psi_N(\boldsymbol{r}_2) \\ \vdots & \vdots & \ddots & \vdots \\ \psi_1(\boldsymbol{r}_N) & \psi_2(\boldsymbol{r}_N) & \cdots & \psi_N(\boldsymbol{r}_N) \end{vmatrix} \qquad II - (08$$

$\frac{1}{\sqrt{N!}}$:is the normalization constant.

Where each wave function ψ_i is called *orbital spin*, because it is composed of two parts: a spatial orbital function and the other is a function of spin (*UP* or *DOWN*).

This gambit is respecting the nature of the electrons (*fermions*).

Then Pauli's principle is respected.

The Slater's determinant is determined using the variational principle.

The application of the Hamiltonian on the wave function gives the energy of Hartree-Fock:

$$E_{HF} = \langle \psi_{SD} | \widehat{H} | \psi_{SD} \rangle =$$

II-(09)

$$\sum_{i=1}^{e} \langle \psi_i | \hat{h} | \psi_i \rangle + \sum_{i=1}^{e} \sum_{j>i}^{e} \left[\iint |\psi_i(\boldsymbol{r}_i)|^2 . \frac{1}{|\boldsymbol{r}_i - \boldsymbol{r}_j|} . |\psi_j(\boldsymbol{r}_j)|^2 . d\boldsymbol{r}_i . d\boldsymbol{r}_j - \iint \psi_i(\boldsymbol{r}_i) . \psi_j^*(\boldsymbol{r}_j) . \frac{1}{|\boldsymbol{r}_i - \boldsymbol{r}_j|} . \psi_j(\boldsymbol{r}_i) . \psi_i^*(\boldsymbol{r}_j) . d\boldsymbol{r}_i . d\boldsymbol{r}_j \right]$$

With :

$$\hat{h} = -\frac{1}{2}\Delta - \sum_{j=1}^{e} \frac{Z_j}{|\boldsymbol{R}_j - \boldsymbol{r}|} \qquad II - (10)$$

This last expression represents the kinetic energy plus the attraction energy between nuclei and electrons. The other two terms are respectively: the integral Coulomb noted J_{ij} (*which is called the integral « the potential » of Hartree*) and the integral exchange rated K_{ij}. The difference between these two terms is the potential energy of Hartree-Fock:

$$V_{HF}(\boldsymbol{r}_i) = \frac{1}{2} \sum_{j>i}^{e} \left[\hat{J}_j(\boldsymbol{r}_i) - \widehat{K}_j(\boldsymbol{r}_i) \right] \qquad II - (11)$$

The implications of the Hartree-Fock approach can be summarized in the following points:

- It obeys Pauli's principle.
- There is no self-interaction.
- It introduces the exchange effect.
- It does not take into account the correlation effect.

II-5. Density Functional Theory (*DFT*)

The main goal of DFT is to replace the multi-electron wave function with the electron density as a base quantity for calculations. While the multi-electron wave function depends on *3N* variables *(where N is the total number of particles in the system),* the density is a function of three variables. It is therefore an easier quantity to deal with both mathematically and conceptually.

II-5-1. DFT framework

DFT allows us to solve the N-body Schrödinger equation involving only the observable $n(\boldsymbol{r})$, defined in the physical space R^3 which substitutes for a configuration space with *3N* variables in which is defined the wave function (*Hartree-Fock*).

The formalism of the DFT is based on the theorem of Hohenberg and Kohn [9]. Before addressing the foundations of DFT, it seems essential to define the central quantity of this theory: "the electron density $n(\boldsymbol{r})$".

II-5-2. Electronic density

Electrons are defined as indistinguishable and inseparable particles. Around this reality, an electron cannot be located as much as an individual particle. Each particle has a probability of presence in an element of volume.

The electronic density $n(\vec{\boldsymbol{r}})$, is the probability of finding one of the *N electrons* in the element of volume $d\vec{\boldsymbol{r}}$. So, it is defined as the multiple integral over the space and spin coordinates of all electrons [10].

$$n(\boldsymbol{r}) = N \int \dots \int |\psi(\boldsymbol{x}_1 \dots \dots \boldsymbol{x}_N)|^2 d\sigma_1 d\sigma_2 dr_2 dr_N \qquad II-(12)$$

II-5-3. Mathematical formulation of the DFT

The quantum many bodies problem obtained after the first level approximation (*Born-Oppenheimer*) is much simpler than the original one, but still far too difficult to be solved.

The approximations developed up to the 60s were all based on the multi-electron wave function. The heaviness of the calculations by these approximations, the imprecision of the results and the performance of the unsuitable means of calculation have pushed researchers towards new methods. In 1964, a new idea was proposed by Walter KOHN and Pierre HOHENBERG which consists in replacing the very bulky multi-electronic wave function, by the electronic density, a simpler and more manageable function. This idea is based on the Thomas-Fermi model (*1927*) [11,12]. This theory was named DFT (*Density Functional Theory*).

II-5-3-1. Hohenberg and Kohn theorem

The traditional formulation of the two theorems [13] of Hohenberg and Kohn is as follows:

II-5-3-1-1. First theorem

The first theorem shows that there is a one-to-one correspondence between the ground-state density $\rho(\vec{r})$ of a many-electron system (*atom, molecule, solid*) and the external potential V_{ext}. And if the total energies have a single minimum for the two potentials, we end up with a contradiction. Another proof was given by Levy [14,15]. Consequently, it demonstrates that the ground state energy of a system with several electrons in the external potential is a unique functional of the electron density $n(\vec{\boldsymbol{r}})$, written as:

$$E[n(\boldsymbol{r})] = \langle\psi|H|\psi\rangle = F_{HK}[n(\boldsymbol{r})] + \int n(\boldsymbol{r})\, V_{ext}(\boldsymbol{r})\, d\boldsymbol{r} \qquad II-(13)$$

Where:

$F_{HK}[n(\boldsymbol{r})] = T_e[n(\boldsymbol{r})] + V_{e\_e}[n(\boldsymbol{r})]$:is the universal functional of Hohenberg and Kohn *(it is said to be universal, because it is common for any electronic system),* since it only depends on the density (*which is determined by the V_{ext} which differs from one system to another*) [16]. This functional is not exactly known.

II-5-3-1-2. Second theorem

The second theorem shows, in accordance with the variational principle, that the total energy functional of any multi-particle system has a minimum which corresponds to the ground state and the density of particles of the ground state.

$$E_0 < E[n(\boldsymbol{r})] \qquad II-(14)$$

Where $n(\boldsymbol{r})$ is the exact electron density of the ground state system.

Unfortunately, the Hohenberg and Kohn functional is not known in practice. This problem can be worked around by approximations. The most widely answered is that of Kohn-Sham.

II-5-3-2. Kohn-Sham approach

The work of Kohn and Sham [17], published in 1965, completes the subsequent work on DFT. Kohn and Sham propose replacing the interacting multi-particle system that obeys the Hamiltonian by an auxiliary system *(without interactions)* that is easier to solve. The Kohn and Sham approach assume that the ground-state electron density of the real system is equal to that of another fictitious system of particles without interactions [18]. This leads to solving a set of equations for independent particles like those of Hartree or Hartree-Fock.

The energy of the ground state of the real system E_0 is written:

$$E_0[n] = T_0[n] + U_0[n] \qquad II-(15)$$

Where:

T_0: the kinetic energy of the real system.

E_0: the electronic contribution to the total ground state energy of the real system.

U_0: the potential energy of the real system (*external and Hartree-Fock*): $U_0 = U_{HF} + U_{ext}$.

Also, the energy of the fictive system is expressed by:

$$E[n] = T[n] + U_H[n] + U_{ext}[n] \qquad II-(16)$$

With: T: The kinetic energy.

U_H: The Hartree potential energy.

U_{ext}: The external potential energy.

E: The electronic contribution to the total energy of the imaginary system.

The subtraction of $II-(15)$ and $II-(16)$ gives:

$$E_0 - E = T_0 - T + (U_{HF} - U_H) \qquad II-(17)$$

This difference is just the electronic correlation energy [18] expressed by:

$$U_C = T_0 - T \qquad II-(18)$$

Also, the exchange energy is written as:

$$U_X = -(U_{HF} - U_H) \qquad II-(19)$$

The exchange and correlation energy can be defined by:

$$U_{XC} = U_C - U_X \qquad II-(20)$$

Substituting $II-(20)$ in $II-(15)$ we find the expression of the energy of the real system:

$$E_0[n] = T[n] + U_H[n] + U_{XC}[n] + U_{ext}[n] \qquad II-(21)$$

The Hohenberg and Kohn universal functional is written as:

$$F_{HK}[n] = T + U_H + U_{XC} \qquad II-(22)$$

By applying the second theorem of Hohenberg and Kohn, the electron density in the ground state is determined using a new Hamiltonian, called Kohn-Sham [18]:

$$H_{KS} = T + U_H + U_{XC} + U_{ext} \qquad II-(23)$$

The Kohn-Sham equation is:

$$H_{KS}\psi_i = \varepsilon_i\psi_i \qquad II-(24)$$

With: ψ_i is the wave function of the i^{th} electréon[4].

So far, the DFT is an exact method but for the DFT and the equations of Kohn Sham become usable in practice, we need to propose a formulation of $E_{XC}[n(\boldsymbol{r})]$ and for that, we must go through an approximation.

II.6. Approximations for the exchange and correlation term

Although the problem of Ne particles in interactions is simplified in an exact way, the knowledge of the true potential of exchange and correlation remains a challenge to be taken up. Much work has to date followed that of Kohn and Sham in order to find an approximate form of the exchange and correlation potential. We will mention the most used. Kohn and Sham considered that density varies slowly in space, so they expressed the exchange and correlation potential using the exchange and correlation energy given by: $\varepsilon_{xc}(n(\boldsymbol{r})) = {}^{\partial E_{xc}}/_{\partial n(\boldsymbol{r})}$. This last one is approximated by the mean field expression:

$$E_{xc}^{LDA}[n] = \int \varepsilon_{xc}(n(\boldsymbol{r}).n(\boldsymbol{r}).d\boldsymbol{r} \qquad II-(25)$$

ε_{xc}: is the exchange and correlation energy density per electron, for a homogeneous gas of electrons.

[4] There is a resemblance between Hartree's (Hartree-Fock) equations and Kohn-Sham's equations although *i* does not have the same physical meaning.

This is known by the local density approximation (LDA). The energy density ε_{xc} is usually calculated using the quantum Monte Carlo method [19].

The LDA has provided this evidence in several areas of solid-state physics and quantum chemistry. This does not exclude a few sudden failures with this approximation [20,21]. To handle the errors of LDA, there have been other approximations, the LSDA (*Local Spin Density Approximation*) [22,23], then the GEA (*Gradient Expansion Approximation*) [24,25] and the GGA (*Generalized Gradient Approximation*) [26,27] where the inhomogeneity of the electron density is taken into account by introducing into the exchange and correlation energy terms depending on the density gradient. The exchange and correlation energy within the framework of the GGA has the general form:

$$E_{xc}^{GGA}[n(\boldsymbol{r})] = \int \varepsilon_{xc}[n(\boldsymbol{r});\ \nabla n(\boldsymbol{r})].n(\boldsymbol{r}).dr \qquad II-(26)$$

There are different GGA methods that take different gradient of the density such as Perdew- Wang (PW91) [28], Perdew-Burke-Ernzerhof (PBE) [29], etc.

Several works were accomplished in the spirit of the LDA and the GGA to obtain a better approximation of E_{xc}Exc, by adding several exact constraints, until the arrival of the meta-GGA [30,31], which is very complex, and some forms of it lack an explicit expression for $\varepsilon_{xc}(n(\boldsymbol{r}))$. Another alternative is to mix the exchange term of the Hartree-Fock model with the correlation functional of the DFT [32,33], the functionals constructed on this principle are qualified as hybrid functionals, but the exchange is over corrected.

II-7. Sampling of the Brillouin zone

For an infinite crystalline solid which is subject to the periodic limits of Born-Vonkarmen [34], resolving the Kohn-Sham equations amounts to find the own functions, which are subjected to an external potential which has the frequency of the crystal, such as:

$$V_{ext}(\boldsymbol{r}) = V_{ext}(\boldsymbol{r}+\boldsymbol{a}) = V_{ext}(\boldsymbol{r}+s.\boldsymbol{a}) \qquad II-(27)$$

With $\boldsymbol{a}$ is the translation vector and s is an integer.

Several terms in the total energy that is calculated can be expressed in integrals on the Brillouin area (*BZ*). On a computer, the integral will be approached by a weighted sum.

The K-Point grid used for this summation must converge and sufficiently dense to properly represent the variations of the integral.

Several methods have been proposed for the choice of the K-Points grid [35,36], but the most used is the method of Monkhorst and Pack [37]. Practically, we must do a convergence study of the physical parameter in question compared to the K points.

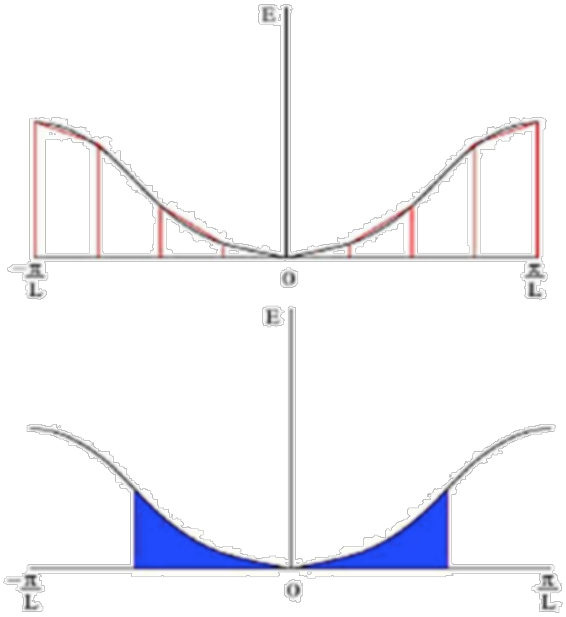

$$E_{tot} = \frac{1}{V}\int_{ZB} E(\boldsymbol{K}).d\boldsymbol{K}$$

$$E_{tot} = \frac{1}{V}\sum_{\boldsymbol{K}} E(\boldsymbol{K})$$

$$n(\boldsymbol{r}) = \frac{1}{V}\int_{ZB} n_{\boldsymbol{K}}(\boldsymbol{r}).d\boldsymbol{K}$$

$$n(\boldsymbol{r}) = \frac{1}{V}\sum_{\boldsymbol{K}} n_{\boldsymbol{K}}(\boldsymbol{r})$$

Fig II.1. The sampling of the first zone of Brillouin.

II.8. The GGA + U method

The DFT +U method is a pragmatic and effective approach for calculating the ground-state properties of strongly correlated systems, and linear-response calculations are widely used to determine the requisite Hubbard [38] parameters from first principles.

GGA and LDA are the mostly used approximations for the exchange-correlation functional. Another approach is GGA+U or LDA+U approach that's based on GGA or LDA type functional with an additional orbital dependent interaction parameter. The interaction parameter is essential for highly localized orbitals as d and f orbitals. The U parameter gives better results than GGA or LDA.

The total energy of the system can be summarized by the following expression [39]:

$$E^{GGA+U} = E^{GGA} + \frac{\bar{U} - \bar{J}}{2} \sum_{\sigma} \left[\left(\sum_{m} n^{\sigma}_{m,m} \right) - \left(\sum_{m,m} n^{\sigma}_{m,m} . n^{\sigma}_{m,m} \right) \right] \qquad II - (28)$$

Thus: $\bar{U}$ and $\bar{J}$: are moderately spherical matrix elements of Coulomb interactions,

And: m : is the occupation matrix of *3d* states obtained by projection of the wave function onto *3d* atomic type states.

→ m or m' = *-2, -1, 0, 1, 2* indicates the different states *d,* while σ = *1* or *-1* indicates the spin.

Note that we express the occupancy matrix in an explicit representation of spin and orbit. An efficient interaction parameter $U_{eff} = \bar{U} - \bar{J}$, or simply U, can be introduced. The calculated total energies are insensitive to $\bar{J}$ when U_{eff} is fixed [40].

II.9. Calculation methods

The purpose of this review is to describe and appraise components of calculation methods, based on the solution of conservation equations in differential form.

II.9.1. The base of plane waves (PW)

plane waves are the exact eigenfunctions of a homogeneous electron gas system. This is the natural choice of the base in the case of simple metals where the ions are seen as a disturbance in an electron gas (*nearly free electron*) [32]. Plane waves are orthonormal and independent of energy, so the Schrödinger equation turns into a simple eigenvalue matrix problem [41]. Another advantage of plane waves is that they are not biased for a particular atom, so all regions in space are treated identically and you don't have to make corrections related to the base superposition, and since plane waves do not depend on atomic positions, then one can apply Hellman Feynman's theorem directly to calculate the forces acting on atoms without having Pulay's terms problem [42].

Plane waves form a '*complete*' basis set; however, they '*never*' converge due to the rapid oscillations of the atomic wave functions close to the nuclei.

The plane wave decomposition of $\varphi_j^k(\boldsymbol{r})$ wave functions consist in expressing these wave functions using the Fourier series:

$$\varphi_j^k(\boldsymbol{r}) = \Omega^{-\frac{1}{2}} \sum_G C_j^k(\boldsymbol{G}) e^{i(\boldsymbol{K}+\boldsymbol{G})\boldsymbol{r}} \qquad II-(29)$$

Plane wave bases, associated with periodic boundary conditions, are often suitable for the study of solids since they by construction satisfy Bloch[5]'s theorem.

The expression of the kinetic energy of the independent particle is very simple, the use of the FFT (*Fast Fourier Transform*) is easy and finally the derivation (*analytical or numerical*) is very easy. But there are two problems that we have to face: the first is that to have a correct representation of the electronic wave function we have to use an infinite number of plane waves, which is impossible. Then the choice of the number of plane waves to use is to truncate by a cut-off energy named E_{cut} such that:

$$\frac{1}{2}|K+G|^2 \leq E_{cut} \qquad II-(30)$$

To determine this very important parameter of calculation one must always make a study of convergence. The second problem is that the valence electron wave function exhibits rapid oscillations near the nucleus, so to have an exact description of these oscillations it is necessary to take many plane waves, something which is academic, to solve this problem we replace the Colombian potential of nuclei and core electrons felt by valence electrons by a pseudo potential [43].

II.9.2. Pseudopotential method (PP)

The pseudopotentials used must satisfy two very important criteria: soft where a reduced number of plane and transferable waves must be used, because the atomic potential used for the generation of the pseudopotential is generally different from the potential of the system studied (molecule, cluster, metal, dielectric, etc.).

The idea behind the use of the pseudopotential is to replace the Colombian potential due to the nucleus felt by the electrons with a more complicated operator which must take into account not only the nuclear potential but also the screening and the repulsion due to the core of the electron (*the frozen core approximation*) and we end up with an effective potential for valence electrons.

[5] Bloch [**] 's theorem is a consequence of the periodicity of the crystal potential, which accounts for the invariance of the system through translational symmetry.

The production of such a pseudopotential (*PP*) begins with a calculation on the isolated atom in question taking into account all these electrons then a PP has extracted analytically in a way that it can regenerate the same spectrum of the potential and the same wave function beyond a radius r_c (*PP cut-off radius*) of the core and inside this sphere, it must be smoother.

The simplest form of the PP is a local multiplicative function [44]. This is why it is called *local*. This form of function leaves few degrees of freedom to adapt the valence states. Often this shape is insufficient for the elements of the first and second columns of the periodic table.

To solve this problem, we add projections of the functions to the local potential. These projections are chosen so that the valence states are orthogonal to the core states. An alternative is to write these projections as a sum over the angular moments with a projection for a value of the quantum number *l* [45,46]. That is why it is called *non-local*. The problem with this formalism is that it can generate non-physical (*ghost*) states [47]. In some cases where a large overlap between core states and valence states, the PP becomes hard. To correct this situation, we introduce a model for the core load in the PP, it gives a better estimate of the load density, especially for the calculation of the energy of exchange and correlation (*Non-Linear Core Corrections)* [48]. All these models are said to be norm-conserving because the charge inside the sphere of radius RC in the PP is the same as in the wave function of the all-electron calculus [49]. In this form of the pseudopotential, the most popular are the PPs of Troullier Martins [50]. To lighten the calculations more, we relax this condition to gain more degrees of freedom which allows us to make the PP softer, this is the idea of Vanderbilt with the *ultrasoft pseudopotentials* USPP [51] and Blöchl with the PAW projector (*augmented plane wave*) [52].

II.9.3. The augmented plane wave method (APW)

Although the pseudopotential method is extremely useful, there are reasons why alternatives could be attractive. Therefore, we will search for a basis set that uses other functions than plane waves, and that does not require the introduction of a pseudopotential. Such a basis set will have to be more efficient, but of course, we do not want it to be biased. Our first example of this will be the *Augmented Plane Wave* (*APW*) basis set. Right from the beginning, it has to be said that the *APW*-method itself is of no practical use anymore today. But for didactical reasons, it is advantageous to discuss *APW* first. The ideas that lead to the *APW* basis set are very similar to what made us introduce the pseudopotential. In the region far away from the nuclei, the electrons

are more or less '*free*'. Free electrons are described by plane waves [53]. Close to the nuclei, the electrons behave quite as they were in a free atom, and they could be described more efficiently by atomic-like functions. Space is therefore divided now into two regions:

- Around each atom a sphere with radius R_α is drawn (*call it* $\boldsymbol{S_\alpha}$). Such a sphere is often called a MT (*Muffin-Tin*) sphere,

- The part of space occupied by the spheres is the muffin tin sphere. The remaining space outside the spheres is called the interstitial region (*call it* $\boldsymbol{I}$).

Therefore, the electron wave function is unfolded according to these two regions on two different bases, namely:

1. Radial Parts and Spherical Harmonics in the MT Sphere,
2. Plane waves in the gap region. Hence, it is called the APW enhanced plane wave method.

One APW used in the expansion of $\phi(r)$ is defined as:

$$\phi(r) = \begin{cases} \varphi_i(\boldsymbol{r}) = \dfrac{1}{\sqrt{\Omega}} \sum_G C_G e^{i(\boldsymbol{k}+\boldsymbol{G})\boldsymbol{r}}, & r > I \\ \varphi_s(\boldsymbol{r}) = \sum_{l,m} A_{l,m} U_l^\alpha(r, E_l) Y_m(\boldsymbol{r}), & r < S_\alpha \end{cases} \qquad II - (31)$$

Where:

α : The atom indexes.

Ω : The unit cell volume.

Y_m : The spherical harmonics.

$A_{l,m}$: The spherical harmonic coefficients.

U_l^α : The radial solution of Schrödinger's equation for the free atom of energy E.

This method is very good for materials with compact structures (*cfc*, *hc* with an ideal *c/a*). It becomes increasingly unreliable with decreasing coordination and symmetry [54]. The main problem with this method is the discontinuity of the wave function on the surface of the MT sphere.

II.9.4. The linearized augmented plane wave method (LAPW)

While the PP-PW method is very efficient and useful, it is always an approximation, and moreover, if we need some information close to the nucleus, such as hyperfine fields or lowest level excitations, we cannot use the PP-PW method. So sometimes we have to do so-called all-electronic "all of this" calculations. For this, we need another basis on which we can project the electron wavefunction. Several methods have been proposed [55,56], but I am interested in the FP-LAPW method.

The basic idea was proposed by Slater [57]. This is of course because the electrons in the inner shell behave like electrons in a single atom.
Therefore, they can be conveniently described by atomic (*orbital*) functions.
Therefore, the potential energy has spherical symmetry and the wave function oscillates.

In the interstitial region away from the nucleus, the electrons are free. They are best described by plane waves.

II.9.5. Density functional perturbation theory (DFPT)

The DFPT method is an established method to study the dynamics of solid-state networks ab initio [58]. Allows computing the system's response to perturbation λ, which is based on a perturbation-dependent extension of the DFT. The linear response provides an analytical method to calculate the second derivative of the total energy with respect to a given disturbance. From the nature of this perturbation, many properties can be calculated, such as the perturbation in the ion position (*atom displacement*) gives the dynamic matrix and phonons, the perturbation of the magnetic field, the perturbation network vector (*strain*) in units, the response is the elastic constant, the perturbation in the electric field, the response is dielectric [59].

DFPT is implemented in the code *ABINIT* [60] to calculate the dynamic matrix, phonon frequency, effective charge, and elastic constant.

II.10. The used codes

For solid systems, many periodic electronic structure calculation programs are currently available and widely used in research and industry, notably CRYSTAL, ABINIT, WIEN2K, VASP, CASTEP,… etc.

II.10.1. General presentation of the code CRYSTAL

The *CRYSTAL* code [61] we used in this work is a quantum chemical program mainly used to calculate the physicochemical properties of crystals (*3D*), plates (*2D*), polymers (*1D*), and molecules or clusters (*0D*). The Theoretical Chemistry Group developed the scheme at the University of Turin in Italy and the Materials Science Modelling Group at Daresbury Laboratory near Warrington, Cheshire, UK. The first version of the code was released in 1988, followed by eight updated versions *CRYSTAL92*, *95*, *98*, *CRYSTAL03*, *06*, *09*, *14*, and *CRYSTAL17*. We used the latest version of "*CRYSTAL17*".

The most common functionalities used to process the physico-chemical characteristics of the system are:

- Geometry optimization.
- Fragment analysis.
- Vibration frequencies.
- Elastic and thermodynamic properties.
- UV-visible, IR and Raman spectra.
- Search for transition states.
- Electronic band structure.

The operation of this program can be separated into certain specific parts which are executed in sequence. In the following the main steps for the calculations of a periodic system are:

- Define input parameters containing all the necessary structural information of the system, the set of bases used and the SCF calculation parameters

(See the structure part of the input file, (Table below)).

- Construct the Bloch basis functions as a linear combination of the local bases of the atomic orbitals.
- Evaluate the Fock (or Kohn-Sham) matrix in real space (F^R) for a local basis.

$$F_{\mu\nu}^{R} = \int \varphi_{\mu}(r)\hat{F}(r)\varphi_{\nu}(r-k)dr \qquad II-(32)$$

$$F_{\mu\nu}^{R} = T_{\mu\nu}^{R} + V_{\mu\nu}^{R} + C_{\mu\nu}^{R} + X_{\mu\nu}^{R} \qquad II-(33)$$

Subscripts μ and ν specify two $AO(\varphi)$ and k is the direct lattice vector.

$T_{\mu\nu}^{R}$*:* The kinetic energy term.

$V_{\mu\nu}^{R}$*:* The term of electron-nucleus interactions.

$C_{\mu\nu}^{R}$*:* The Coulomb electron-electron interaction term.

$X_{\mu\nu}^{R}$: The term of exchange interactions.

- Represent the Fock matrices $F_{\mu\nu}^{R}$ in the basis set of the Bloch function at each point k in the reciprocal space by the Fourier transform, then diagonalize them to obtain the eigenvalues and eigenvectors and solve the Fock matrix equation $II-(32)$.
- Determine the Fermi energy (*the highest occupied state of the system in the first BZ*) and construct a new density matrix in direct space.
- Determine the total energy of the system (*per mesh*), E_{tot}, and reconstruct the Fock (*or Kohn-Sham*) matrices, repeating the steps following an iterative cycle until convergence is achieved (*self-consistent field calculation, SCF*). In *CRYSTAL17* this is determined by the total energy difference between successive cycles reaching the threshold specified in the input file.
- Finally, the converged wave function of the SCF procedure can be used to calculate various properties such as density of states, band structure, and charge densities.

The input file in the *CRYSTAL17* includes a title and three sections (called "blocks"). Each block is made up of the keywords and the numeric parameters. Each block ends with the END (mandatory) or STOP keyword. The latter will cause the execution to stop immediately. Optional keywords may be present within each section. Detailed information about the input functions can be found in the "*CRYSTAL User's Manual*" [62].

Table II.2: Input parameters in a file input.

	NAME
BLOCK 1	**GEOMETRICAL DATA** • Standard geometric parameters (the space group, the atomic coordinates ... etc.) • Optional keywords. **END**
BLOCK 2	**BASE SET** • Standard basic functions or with PP. • Optional keywords. **END**
BLOCK 3	**DFT** • Choice of approximation. • Optional keywords. **END**
BLOCK 4	**SCF CALCULATION AND CONTROL PARAMETERS** • Choice E_{xc} • SHRINK factor (*number of points k in reciprocal space*) • Maximum number of SCF cycles • Optional keywords. **END**

II.10.2. General presentation of the code CASTEP

CASTEP (*Cambridge Serial Total Energy Package*) [63]. This code was originally developed in 1988 by Payne et *al.* It is an ab-initio computer code and it is part of a set of digital simulation software called Materials Studio which is marketed by *Dassault Systèmes Biovia*©. CASTEP is developed in the Condensed Matter Theory group at the University of Cambridge, UK. It is a program that uses Density Functional Theory (*DFT*) to simulate the properties of solids. CASTEP can predict physical properties including elastic constants, structural properties, energy

band diagrams, electronic densities of states, charge densities and optical properties as well as vibrational and thermodynamic properties.

This code is used to simulate the total energy by special integration of the points in the first *BZ* with a plane wave basis for the expansion of the wave functions, in this zone being carried out on a finite set of points k produced by the method of Monkhorst and Pack.
CASTEP runs on Windows and Linux. A graphical interface compliant with Microsoft Windows standards, allows the user to interact with *3D* graphical models, configure calculations and analyze results through dialog boxes that are simple and familiar to any Windows user.

II-11. The elastic properties

Elasticity is concerned with the relationship between the stresses and deformations that a solid experience when subjected to external forces.
It is connected to a number of important variables of the solid state, including the melting point, the Debye temperature, the specific heat, the thermal expansion, the equation of state (*EOS*), and others [64].

II-11-1. Tensors of elastic constants

II-11-1-1. The tensor of constraints

By definition, the constraint is the force acting on the solid's surface unit. A matrix (*9 components*) is also used to depict the stress tensor that has been mentioned [65].

$$\sigma = \begin{pmatrix} \sigma_{xx} & \sigma_{xy} & \sigma_{xz} \\ \sigma_{yx} & \sigma_{yy} & \sigma_{yz} \\ \sigma_{zx} & \sigma_{zy} & \sigma_{zz} \end{pmatrix} = \begin{pmatrix} \sigma_{11} & \sigma_{12} & \sigma_{13} \\ \sigma_{21} & \sigma_{22} & \sigma_{23} \\ \sigma_{31} & \sigma_{32} & \sigma_{33} \end{pmatrix} \qquad II-(33)$$

In the notation σ_{ij} the subscript i indicates the direction of the force, and the subscript j refers to the normal to the plane on which the force is applied (see Figure I.3, below), for example the stress σ_{xy} is the force applied in the direction x on a unit area of a plane who's normal is y.

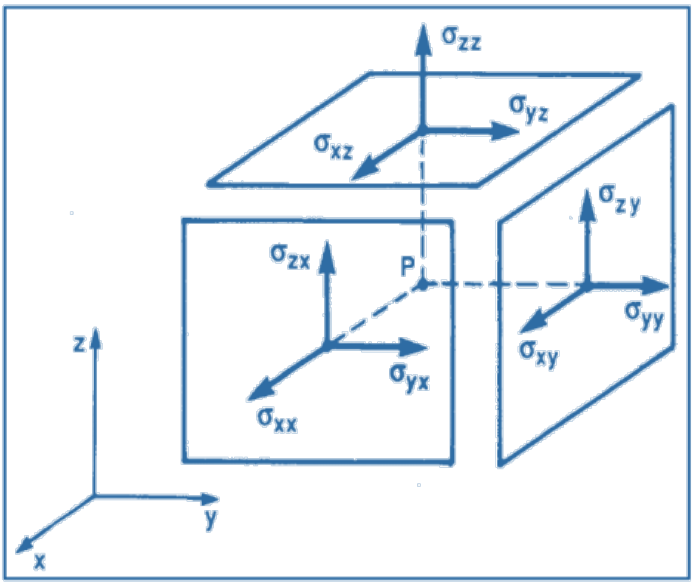

Fig II-2. The components of the stress tensor [35].

Due to the symmetry of the stress tensor, $\sigma_{ij} = \sigma_{ji}$ the number of their independent components reduces to 6.

The components σ_{ii} are called normal stresses (*traction or compression),* because they act perpendicular to a facet of normal P_x, P_y or P_z.

• Three normal components σ_{11}, σ_{22} and σ_{33}.

The elements $\sigma_{ij}$with $i \neq j$ are the tangential (*shear*) stresses since they act in the plane of the surface. The stress components have the dimension of a force per unit area or an energy per unit volume.

• Three tangential components $\sigma_{12} = \sigma_{21}$, $\sigma_{13} = \sigma_{31}$ and $\sigma_{23} = \sigma_{32}$.

II-11-1-2. The deformation tensor

Deformation is the alteration of a solid's volume or shape caused by external forces without a change in the solid's mass. When an item is at its rest position, which is the starting point from which deformations are measured, no force is applied on the object [66].

$$\varepsilon = \begin{pmatrix} \varepsilon_{xx} & \varepsilon_{xy} & \varepsilon_{xz} \\ \varepsilon_{yx} & \varepsilon_{yy} & \varepsilon_{yz} \\ \varepsilon_{zx} & \varepsilon_{zy} & \varepsilon_{zz} \end{pmatrix} = \begin{pmatrix} \varepsilon_{11} & \varepsilon_{12} & \varepsilon_{13} \\ \varepsilon_{21} & \varepsilon_{22} & \varepsilon_{23} \\ \varepsilon_{31} & \varepsilon_{32} & \varepsilon_{33} \end{pmatrix} \qquad II-(34)$$

The elements of the strain tensor ε_{ij} are generally defined by the following relation [34]:

$$\varepsilon_{ij} = \frac{1}{2}\left(\frac{\partial u_i}{\partial x_j} + \frac{\partial u_j}{\partial x_i}\right) \qquad II-(35)$$

The elongations (*or compressions*) shown by the diagonal components of the ε_{ii} tensor are changes in length in the x, y, or z directions. The shear strains ε_{ij}, on the other hand, are changes in the angles between the axes P_x, P_y, and P_z. Since the strain's components are ratios of lengths, they have no dimensions.

II-11-2. Case of a monoclinic system

Systems with monoclinic symmetry have *13* independent elastic constants: $C_{11}, C_{22}, C_{33}, C_{44}, C_{55}, C_{66}, C_{12}, C_{13}, C_{16}, C_{23}, C_{26}, C_{36}$ et C_{45} [67].

$$\begin{pmatrix} C_{11} & C_{12} & C_{13} & 0 & 0 & C_{16} \\ C_{12} & C_{22} & C_{23} & 0 & 0 & C_{26} \\ C_{13} & C_{23} & C_{33} & 0 & 0 & C_{36} \\ 0 & 0 & 0 & C_{44} & C_{45} & 0 \\ 0 & 0 & 0 & C_{45} & C_{55} & 0 \\ C_{16} & C_{26} & C_{36} & 0 & 0 & C_{66} \end{pmatrix} \qquad II-(36)$$

II-11-2-1. Mechanical stability

One of the most common types of instabilities in crystals is the so-called mechanical instability when one or more elastic constants (*or their special combinations*) tend to zero. Consideration of the mechanical stability of the crystal lattice was originally formulated by Born and Huang [68, 69], who showed that by expanding the internal energy of a crystal into a power series of stresses, it is possible to obtain stability criteria in terms of conditions on the elastic constants while considering the positive energy. Thus a necessary condition for mechanical stability is that the matrix of elastic constants is positively defined (*Born's criterion*). A matrix is positively defined if the determinants of the matrices of successive orders that compose it are all positive. The condition of dynamic or mechanical stability of a network implies that the variation

of energy under any small deformation is positive. This condition can be formulated in terms of elastic constants C_{ij} [70].

• For a monoclinic system, the mechanical stability criteria are given by the following relations [71, 72]:

$C_{11} > 0, C_{22} > 0, C_{33} > 0, C_{44} > 0, C_{55} > 0, C_{66} > 0,$

$(C_{33}C_{55} - {C_{35}}^2) > 0, (C_{44}C_{66} - {C_{46}}^2) > 0, (C_{22}+C_{33} - 2C_{23}) > 0,$

$[C_{11} + C_{22} + C_{33} + 2(C_{12} + C_{13} + C_{23})] > 0,$

$\left[C_{22}\left(C_{33}C_{55} - {C_{35}}^2\right) + 2C_{23}C_{25}C_{35} - {C_{23}}^2C_{55} - {C_{25}}^2C_{33})\right] > 0,$

$\{2[C_{15}C_{25}(C_{33}C_{12} - C_{13}C_{23}) + C_{15}C_{35}(C_{22}C_{13} - C_{12}C_{23}) + C_{25}C_{35}(C_{11}C_{23} - C_{12}C_{13})] -$

$\left[{C_{15}}^2\left(C_{22}C_{33} - {C_{23}}^2\right) + {C_{25}}^2\left(C_{11}C_{33} - {C_{13}}^2\right) + {C_{35}}^2\left(C_{11}C_{22} - {C_{12}}^2\right) + C_{55}g\right]\} > 0,$

$$g = C_{11}C_{22}C_{33} - C_{11}{C_{23}}^2 - C_{22}{C_{13}}^2 - C_{33}{C_{12}}^2 + 2C_{12}C_{13}C_{23} \qquad II-(37)$$

II-11-2-2. Voigt's method (Voigt, 1928)

In the case of the Voigt hypothesis [73], the strain is assumed to be constant throughout the polycrystal and equal to the macroscopic strain applied to the sample. This amounts to taking an average over the elastic moduli C_{ij}.

$$C^{Voigt} = \bar{C} \qquad II-(38)$$

Where the bar indicates an average over the whole orientation space. In this approach, the compressibility modulus and the shear modulus are expressed as a function of the following general expressions [74]:

$$B^{Voigt} = \frac{1}{9}(C_{11} + C_{22} + C_{33} + 2C_{12} + 2C_{13} + 2C_{23}) \qquad II-(39)$$

$$G^{Voight} = \frac{1}{15}[C_{11} + C_{22} + C_{33} - (C_{12} + C_{13}+C_{23})] + \frac{3}{15}(C_{44} + C_{55} + C_{66}) \qquad II-(40)$$

II-11-2-3. Reuss's method (Reuss, 1929)

In the Reuss hypothesis [75], the stress is assumed to be constant throughout the polycrystal and equal to the macroscopic stress. The average is taken from the deformability coefficients S_{ij}.

$$S^{Reuss} = \bar{S} \qquad II-(41)$$

In the Reuss approach, the two moduli of elasticity B and G are given as a function of the deformability constants as follows:

$$(B^{Reuss})^{-1} = (S_{11} + S_{22} + S_{33}) + 2(S_{12} + S_{13} + S_{23}) \qquad II-(42)$$

$$(G^{Reuss})^{-1} = \frac{1}{15}[4(S_{11} + S_{22} + S_{33}) - 4(S_{23} + S_{13} + S_{12}) + 3(S_{44} + S_{55} + S_{66})] \; II-(43)$$

II-11-2-4. Hill's method (Hill, 1952)

Hill [76-77] showed that the method of Voigt and that of Reuss give the limits between which the real elastic moduli of the polycrystal are situated; the modulus of a polycrystalline solid is necessarily included between the two moduli (*that of Voigt and that of Reuss*). The Voigt's modulus being the upper limit and the Reuss' modulus the lower limit. He also observed that the average value of these quantities gives results close to the values measured experimentally. The real values of the isotropic elastic constants:

$$C^{Hill} = \frac{C^{Voigt} + C^{Reuss}}{2} \text{ and } S^{Hill} = \frac{S^{Voigt} + S^{Reuss}}{2}$$

The actual moduli of elasticity, *B* and *G*, approximated by Hill's mean are given by:

$$B^{Hill} = \frac{B^{Voigt} + B^{Reuss}}{2} \text{ and } G^{Hill} = \frac{G^{Voigt} + G^{Reuss}}{2}$$

For systems possessing monoclinic symmetry B and G, in Voigt's approach are given by the following expressions:

$$B^{Voigt} = \frac{1}{9}(2C_{11} + 2C_{22} + 4C_{13} + C_{33}) \qquad II-(44)$$

$$G^{Voigt} = \frac{1}{30}(7C_{11} + 5C_{12} + 4C_{13} + 2C_{33} + 12C_{44}) \qquad II-(45)$$

In Reuss' approach, these two moduli are expressed in terms of the C_{ij} as follows:

$$B^{Reuss} = \frac{(C_{11} + C_{12})C_{33} - 2{C_{13}}^2}{C_{11} + C_{12} - 4C_{13} + 2C_{33}} \qquad II-(46)$$

$$G^{Reuss} = \frac{15}{2}\left[\frac{2C_{11} + 2C_{12} + 4C_{13} + C_{33}}{C_{33}(C_{11} + C_{12}) - 2C_{13}^{\ 2}} + \frac{3C_{11} - 3C_{12} + 6C_{44}}{C_{44}(C_{11} - C_{12}) - 2C_{14}^{\ 2}}\right]^{-1} \qquad II-(47)$$

II-11-2-5. Poisson's Ratio

The Poisson's ratio X characterizes the traction and compression of the solid perpendicular to the direction of the applied force. In the case of a cubic system, the Poisson's ratio is defined as:

$$\nu = \frac{3B - 2G}{2(3B + G)} \qquad II-(48)$$

II-11-2-6. Debye Temperature and Elastic Wave Speeds

One of the most important parameters that determines the thermodynamic properties of materials (the specific heat and the melting temperature...etc.) is the Debye temperature. Generally, a high value of Θ_D reveals high thermal conductivity and melting temperature.

The Debye temperature can be derived from isotropic acoustic wave velocities which are in turn related to isotropic moduli of elasticity [78]. It is described as the temperature at which the solid's atoms vibrate in all of their potential modes. The acoustic modes dominate the vibrational characteristics at low temperatures:

$$\Theta_D = \frac{h}{k_B}\left[\frac{3n}{4\pi}\left(\frac{N_A\rho}{M}\right)\right]^{1/3} v_m \qquad II-(49)$$

Such that h is Planck's constant, k_B is the Boltzmann constant, n is the number of atoms per molecule, N_A is Avogadro's number, M the molecular weight and v_m average speed of sound.

According to the elastic grades B and G, the average speed of sound v_m, the speed of transverse elastic waves v_s, and longitudinal elastic waves v_l in a solid depend on the density ρ of the solid in the following manner:

$$v_m = \left[\frac{1}{3}\left(\frac{2}{v_p^3} + \frac{1}{v_s^3}\right)\right]^{-1/3} \qquad II-(50)$$

$$v_p = \left[\left(B + \frac{4G}{3}\right)\Big/\rho\right]^{1/2} \qquad II-(51)$$

$$v_s = \sqrt{G/\rho} \qquad II-(52)$$

II-11-3. Elastic anisotropy

The elastic anisotropy represents the dependence of the elastic response of crystalline material on the direction of stress. It is defined in our study by four different approaches.

The graphical representation of a three-dimensional surface diagram of the directional dependence of the elastic moduli is a practical and simple method for detecting elastic anisotropy. The position vectors of each point on this surface serve as references, and each position vector's modulus denotes the value of the elastic quantity measured in the direction indicated by the director cosines in the vector's spherical coordinates. In the case of a material with monoclinic symmetry, the directional dependence of Young's modulus E and linear compressibility B is given by [79]:

$$E = [S_{11}l_1^4 + 2S_{12}l_1^2l_2^2 + 2S_{13}l_1^2l_3^2 + 2S_{15}l_1^3l_3 + S_{11}l_1^4 + S_{22}l_2^4 + 2S_{23}l_2^2l_3^2 + 2S_{25}l_1l_2^2l_3 + S_{33}l_3^4 + 2S_{35}l_2l_3^3 + S_{44}l_2^2l_3^2 + 2S_{46}l_1l_2^2l_3 + S_{55}l_1^2l_3^2 + S_{66}l_1^2l_2^2]^{-1} \qquad II-(52)$$

$$B = (S_{11} + S_{12} + S_{13})l_1^2 + (S_{12} + S_{22}+S_{23})l_2^2 + (S_{13}+S_{23} + S_{33})l_3^2 + (S_{15}+S_{25}+S_{35})l_3l_1 \qquad II-(53)$$

• S_{ij} are the material's deformability constants, while l_i are the direction cosines of the direction, which are given in spherical coordinates by:

$$\begin{cases} l_1 = \cos(\varphi)\sin(\theta) \\ l_2 = \sin(\varphi)\sin(\theta) \\ l_3 = \cos(\theta) \end{cases} \qquad II-(54)$$

• Any variation from the ideal spherical shape (*deformed surface*) implies some degree of anisotropy in the modulus of elasticity, whereas a perfect spherical shape shows isotropic behavior (*no directional dependence*).

II-12. Optical properties

The area of physics known as **optics** studies processes related to light. It is very interesting to understand the various ways that light interacts with materials in solid state physics, such as absorption, transmission, reflection, scattering, and emission. We can now better comprehend the electrical characteristics of materials thanks to the study of the optical properties of solids.

II-12-1. The dielectric function

When exposed to an electromagnetic wave's oscillating electric field, a material's optical response is described by its dielectric function $\varepsilon(\omega, k)$. This physical quantity is based on the

electronic transitions between the valence bands and the conduction bands in the material under examination, which strongly depends on the structure of the material's energy bands. It is supplied by, and has two parts: one that is actual and the other that is made up of [80]:

$$\varepsilon(\omega) = \varepsilon_1(\omega) + i\varepsilon_2(\omega) \qquad II-(55)$$

The imaginary part of the function is calculated in the dipole approximation from the matrix of transitions between occupied valence states and conduction states using the following formula:

$$\varepsilon_2(\omega) = \frac{2\pi e^2}{m_e^2 \omega^2 \varepsilon_0} \sum_{c,v} \int_{BZ} |\langle \Psi_k^c | u.r | \Psi_k^v \rangle|^2 \delta(E_k^c - E_k^v - \hbar\omega) dk^3 \qquad II-(56)$$

In reality, the two, real $\varepsilon_1(\omega)$ and imaginary $\varepsilon_2(\omega)$, parts of the dielectric function are not independent of each other. Indeed, by using the Kramers-Kronig [81] connection, one may be inferred to know the other.

$$\varepsilon_1(\omega) = 1 + \frac{2}{\pi} P \int_0^\infty \frac{\omega' \varepsilon_2(\omega')}{(\omega')^2 - \omega^2} d\omega' \qquad II-(57)$$

$$\varepsilon_2(\omega) = -\frac{2}{\pi} P \int_0^\infty \frac{\varepsilon_1(\omega') - 1}{(\omega')^2 - \omega^2} d\omega' \qquad II-(58)$$

Where ω is the frequency and P the principal part of the Cauchy integral.

II-12-2. The refractive index

The refractive index $n(\omega)$ of a material is defined by the ratio of the speed of light in vacuum c to the speed of light in material v according to:

$$n = \frac{c}{v} \qquad II-(59)$$

The refraction of an environment can be described by a single quantity called the complex refractive index. It is usually presented by the symbol $\tilde{n}$ defined by the equation:

$$\tilde{n} = n + ik \qquad II-(60)$$

The real part of $\tilde{n}$, namely n, is the same as the normal incidence refractive index. The imaginary part of $\tilde{n}$, namely k, is called the extinction coefficient. The two quantities are linked to the dielectric function by the following two relations [82]:

$$n(\omega) = \frac{1}{\sqrt{2}}\left[\sqrt{{\varepsilon_1}^2(\omega)+{\varepsilon_2}^2(\omega)} + \varepsilon_1(\omega)\right]^{\frac{1}{2}} \qquad II-(61)$$

$$k(\omega) = \frac{1}{\sqrt{2}}\left[\sqrt{{\varepsilon_1}^2(\omega)+{\varepsilon_2}^2(\omega)} - \varepsilon_1(\omega)\right]^{\frac{1}{2}} \qquad II-(62)$$

II-12-3. The absorption coefficient

The absorption coefficient $\alpha(\omega)$ indicates the fraction of energy lost by the wave as it passes through the material. It can be defined in terms of the extinction coefficient $k(\omega)$ by the following relation [83]:

$$\alpha(\omega) = \frac{4\pi}{\lambda}k(\omega) \qquad II-(63)$$

Where λ represents the wavelength of light in vacuum.

II-12-3. The reflectivity

The reflection of radiation from a surface is described by the reflection coefficient or reflectivity. This is usually denoted by the symbol $R(\omega)$ and is defined as the ratio of reflected intensity to incident intensity on the surface [84], this property defines the colors of metals. The reflectivity is calculated from the refractive index and the extinction coefficient by the following relation [80]:

$$R(\omega) = \frac{n+ik-1}{n+ik+1} \qquad II-(64)$$

II-13. Conclusion

In this chapter, we have seen the equations used and the different approximations for their resolution. Among these methods, we insisted on the theory of functional density with particular attention to the interpretation of its bases. We have shown that the essential difficulty comes from the formulation of the correlation exchange functional which has generated several types of approximations whose evolution has been deemed beneficial to be presented here. We have briefly introduced the different types of essential functions used and studied properties.

II. References

[1]. E. Schrodinger. (Erste Mitteilung). Ann. Physik 79, (1926) 361.

[2]. E. Schrodinger. (Zweite Mitteilung). Ann. Physik 79, (1926) 489.

[3]. E. Schrodinger. (Vierte Mitteilung). Ann. Physik 81, (1926) 109.

[4]. E. Schrodinger. The Physical Review, 28, (1926), 1049.

[5]. M. Born, J. R. Oppenheimer. Ann Phys. 87, (1927) 457.

[6]. D. R. Hartree. Proc : Combridge Philos. Soc 24, (1928) 89.

[7]. V. Fock. Z. Phys. 61, (1930) 795.

[8]. J. C. Slater. Phys Rev. 34, (1929) 1293.

[9]. Hohenberg, P. and W. Kohn, *Inhomogeneous electron gas.* Physical review, 1964. **136**(3B): p. B864.

[10]. Gross, E. and R. Dreizler, *Density functional theory: an approach to the quantum many-body problem*. 1990, Springer, Berlin.

[11]. L. H. Thomas. Proc. Combridge Phil. Soc 23, (1927) 542.

[12]. E. Fermi. Rend. Accad. Naz. Lincei 6, (1927) 602.

[13]. P. Hohenberg, W. Kohn. Phys. Rev B,136, (1964) 864.

[14]. M. Levy. Proc. Natl. Acad. Sci. 76, (1979) 6062.

[15]. M. Levy and J. P. Perdew, in Density Functional Methods in Physics, edited by R. M. Dreizler and I. daProvidencia, Plenum, New York, 1985, p. 11.

[16]. E. Kaxiras. Atomic and Electronic Structure of Solids, Cambridge University Press, New York, 2003, p 60.

[17]. W. Kohn, L. J. Sham. Phys. Rev 140, (4A) (1965) 1133.

[18]. R. M. Martin. Electronic Structure Basic Theory and Practical Methods, Combridge University Press, New York, 2004, p. 135.

[19]. D.M. Ceperley, B.J. Alder. Phys. Rev. Lett. 45, (1980) 566.

[20]. P. L. Taylor, O. Heinonen. A Quantum Approach to Condensed Matter Physics, Cambridge University Press, New York, 2004, p. 191.

[21]. P. Flude. Electron Correlations in Molecules and solids. Berlin; Heidelberg; New York: Springer, 1995, p. 49.

[22]. U. V. Barth, L. Hedin. J. Phys. C 5, (1972) 1629.

[23]. A. K. Rajagopal, J. Callaway. Phys. Rev B. 7, (1973) 1912.

[24]. F. Herman, J. p. Van Dyke, I. P. Ortenberger. Phys. Rev Lett. 22, (1969) 807.

[25]. P. S. Svendsen, U. V. Barth. Phys. Rev B. 54, (1996) 17402.

[26]. D. C. Langreth, M. J. Mehl. Phys. Rev. Lett. 47, (1981) 446.

[27]. J. P. Perdew. Phys. Rev. B 33, (1986) 8822.

[28]. J. P. Perdew and Y. Wang, "Accurate and simple analytic representation of the electron-gas correlation energy," Phys. Rev. B, vol. 45, no. 23, pp. 13244– 13249, Jun. 1992.

[29]. J. P. Perdew, K. Burke, and M. Ernzerhof, "Generalized Gradient Approximation Made Simple," Phys. Rev. Lett., vol. 77, no. 18, pp. 3865–3868, Oct. 1996.

[30]. M. Filatov, W. Thiel. Phys. Rev. A 57, (1998) 189.

[31]. J.P. Perdew, S. Kurth, A. Zupan, P. Blaha. Phys. Rev. Lett. 82, (1999) 2544.

[32]. A. D. Becke. J. Chem. Phys. 98, (1993) 5648.

[33]. C. Lee, W. Yang, and R.G. Parr. Phys. Rev. B 37, (1988) 785.

[34]. N. W. Ashcroft, N. D. Mermin. "Solid State Physics". Saunders College Publishing. 1976.

[35]. A. Baldereschi. Phys. Rev. B 7, (1973) 5212.

[36]. D.J. Chadi, M.L. Cohen. Phys. Rev. B 8, (1973) 5747.

[37]. H. J. Monkhorst, J.D. Pack. Phys. Rev. B 13, (1976) 5188.

[38]. Tancogne-Dejean, Nicolas, and Angel Rubio. "Parameter-free hybridlike functional based on an extended Hubbard model: DFT+ U+ V." *Physical Review B* 102.15 (2020): 155117.

[39]. Wang, Lei, Thomas Maxisch, and Gerbrand Ceder. "Oxidation energies of transition metal oxides within the GGA+ U framework." *Physical Review B* 73.19 (2006): 195107.

[40]. Dudarev, S. L., et al. "Electron-energy-loss spectra and the structural stability of nickel oxide: An LSDA+ U study." *Physical Review B* 57.3 (1998): 1505.

[41]. B. Meyer. NIC Series, Vol. 31, ISBN 3-00-017350-1, pp. 71-83, 2006.

[42]. P. Pulay. Mol. Phys. 197, (1969) 17.

[43]. Singh, David J., and Lars Nordstrom. *Planewaves, Pseudopotentials, and the LAPW method*. Springer Science & Business Media, 2006.

[44]. J. Harris, R. O. Jones. Phys. Rev.Lett. 41, (1978) 191.

[45]. J.C. Phillips, L. Kleinman. Phys. Rev. Lett. 116, (1959) 287.

[46]. G. B. Bachelet, D. R. Hamann, M.Schlüter. Phys. Rev. B 26, (1982) 4199.

[47]. X. Gonze, R. Stumpf, M. Schefler. Phys. Rev. B 44, (1991) 8503.

[48]. S. G. Louie, S. Froyen, M. L. Cohen. Phys. Rev. B 26, (1982) 1738.

[49]. D.R.Hamann, M. Schlüter, C. Chiang. Phys. Rev. Lett 43, (1979) 1494.

[50]. N. Troullier, J. L. Martins. Phys. Rev. B 43, (1991) 1993.

[51]. D. Vanderbilt. Phys. Rev. B 41, (1990) 7892.

[52]. P. E. Blöchl. Phys. Rev. B 50, (1994) 17953.

[53]. Cottenier, Stefaan. "Density Functional Theory and the family of (L) APW-methods: a step-by-step introduction." *Instituut voor Kern-en Stralingsfysica, KU Leuven, Belgium* 4.0 (2002): 41.

[54]. N. Elyashar. D.D. Koelling. Phys. Rev. B 13, (1976) 5362.

[55]. J. Korringa. Physica. 13, (1947) 392.

[56]. W. Kohn, N. Rostoker. Phys. Rev. 94, (1954) 1111.

[57]. J. C. Slater. Phys. Rev. 51, (1937) 846.

[58]. Pouillon, Y. *What is Abinit*. 2014 2014/06/02; Available from: https://wiki.abinit.org/doku.php#dokuwiki_top.

[59]. Wolfram, Thomas, and Sinasi Ellialtioglu. *Electronic and optical properties of d-band perovskites*. Cambridge University Press, 2006.

[60]. http://www.sers.york.ac.uk/~mijp1/teaching/grad-FPMM/practical-classes/MS- CASTEP - guid.

[61]. R. Dovesi, A. Erba, R. Orlando, C.M. Zicovich-Wilson, B. Civalleri, L. Maschio, M. Rérat, S. Casassa, J. Baima, S. Salustro, B. Kirtman, Quantum-mechanical condensed matter simulations with CRYSTAL, Wiley Interdisciplinary Reviews: Computational Molecular Science. 8 (2018) 1–36. doi:10.1002/wcms.1360.

[62]. R. Dovesi, A. Erba, R. Orlando, C.M. Zicovich-Wilson, B. Civalleri, L. Maschio, M. Rerat, S. Casassa, J. Baima, B. Salustro, B. Kirtman, CRYSTAL17 User's Manual, (2017).

[63]. Segall, M., et al., *First-principles simulation: ideas, illustrations and the CASTEP code.* Journal of Physics: Condensed Matter, 2002. **14**(11): p. 2717.

[64]. N. CHOUIT: « Etude ab-intio des différentes propriétés structurales, électroniques, optiques et thermiques des composés ternaires (CaLiF3 et SrLiF3) par la méthode FP-LAPW», Thèse de Doctorat, Université de ANABA, 2014.

[65]. Pavlov, A. Khokhlov. Physique du solide. Ed. Mir, Moscou, 416, 1989.

[66]. C. Kittel, Introduction à la physique de l'etat solide. Dunod. 1972.

[67]. F. Mouhat and F. X Coudert, Phys. Rev. B 90, 224104 (2014).

[68]. M. Born, Proc. Cambridge Philos. Soc., 36, 160 (1940).

[69]. M. Born et K. Huang, Dynamical Theory of Crystal Lattices, Clarendon, Oxford (1956).

[70]. Z. Wu, E. Zhao, H. Xiang, X. Hao, X. Liu, J. Meng, Phys. Rev. B 76, 054115 (2007).

[71]. S. Goumri-Said, M.B. Kanoun, Comput. Matter Sci. 43, 243 (2008).

[72]. W.Voigt, Lehrburch der Kristallphysik. Leipzig: Teubner; (1928).

[73]. E. Schreiber, O. L. Anderson et N. Soga, Elastic constants and their measurement (McGraw-Hill, Inc. (1973) USA).

[74]. A. Reuss, Z. Angew, Math. Mech. 9, 49 (1929).

[75]. R. Hill, Proc. Phys. Soc. A 65, 349 (1952).

[76]. R. J. Hill, Mech. Phys. Solids 11, 357 (1963).

[77]. R. Hill, Proc. Phys. Soc. London 65, 396 (1952).

[78]. P. Wachter, M. J. Filzmoser and Rebizant, *Physica. B*. 2001, 293, 199.

[79]. J.F. Nye, Properties of Crystals, Oxford University Press, 1985.

[80]. Hosseini, S., T. Movlarooy, and A. Kompany, *First-principles study of the optical properties of PbTiO3.* The European Physical Journal B-Condensed Matter and Complex Systems, 2005. **46**(4): p. 463-469.

[81]. 尾中龍猛, *F. Wooten: Optical Properties of Solids, Academic Press, New York and London, 1972, 260 ページ, 23.5× 16cm, 4,660* 円. 日本物理學會誌, 1973. **28**(9): p. 803-804.

[82]. Saha, S., T. Sinha, and A. Mookerjee, *Structural and optical properties of paraelectric SrTiO3.* Journal of Physics: Condensed Matter, 2000. **12**(14): p. 3325.

[83]. Goubin, F., *Relation entre fonction diélectrique et propriétés optiques: application à la recherche d'absorbeurs UV inorganiques de deuxième génération*. 2003, Université de Nantes.

[84]. Dupeux, M., *AIDE-MEMOIRE SCIENCE DES MATERIAUX,© Dunod.* REPUBLIQUE ALGERIENNE DEMOCRATIQUE ET POPULAIRE MINISTERE DE L'ENSEIGNEMENT SUPERIEUR ET DE LA RECHERCHE SCIENTIFIQUE REPUBLIQUE ALGERIENNE DEMOCRATIQUE ET POPULAIRE MINISTERE DE L'ENSEIGNEMENT SUPERIEUR ET DE LA RECHERCHE SCIENTIFIQUE, 2004.

[* *]. F. Bloch. Z. Phys. 52, (1928) 555.

→ *"Energy is liberated matter, matter is energy waiting to happen."...*

CHAPTER -III-

Results and discussion

The physics of matter aims to describe and explain the properties of materials that are unknown before using them.

III-1. Introduction

In this chapter, we will present and discuss the results of our calculations on the structural, electronic, elastic, and optical properties of the ternary compounds $CsBSe_3$ and $TlBSe_3$ in the monoclinic structure carried out in the context of the DFT. The calculations were carried out with the *CASTEP* code [1] using the PW method and the ultra-soft PP method introduced by Vanderbilt [2], in addition to the combinations of atomic orbitals (*CLOA*) implanted in the *CRYSTAL* code [3].

III-2. Calculation details

The potential for exchange and correlation has been dealt with in the generalized gradient approximation (*GGA*) parameterized by Perdew-Burk-Ernzerhof (*PBE*) [4]. The parameters of the calculations conducted in this predictive study on all the physical properties considered have been carefully examined. In CASTEP, the sampling of the *BZ* is done by Monkhorst Pack [5].

The valence states considered are: $B: 2s^2\ 2p^1$

$Se: 4s^2\ 4p^4$

$Cs: 5s^2\ 5p^6\ 6s^1$

$Tl: 5d^{10}\ 6s^2\ 6p^1$

III-3. Geometric crista-optimization

$ABSe_3$ materials crystallize in the monoclinic structure of the perselenoborate family (*see chapter I*) with space group $P2_1/c$ (*ranked 14 in the international table of crystallography*) and Cc (*ranked 9 in the international table of crystallography*) for $CsBSe_3$ and $TlBSe_3$ respectively.

III-4. Convergence testing

Before calculating the physical properties of the system in its ground state, it is necessary to optimize the equilibrium geometry of the system with a good choice of convergence parameters. Thus, the size of the plane wave basis on which the pseudo wave functions of Kohn and Sham are developed (the cutoff energy E_{cut}) and the sampling of the first *BZ* (the point number *k*) are optimized.

III-4-1. Choice of the basic size of the wave functions (cut-off energy)

The Kohn-Sham orbitals are decomposed on a plane wave basis, this last decomposition consists in expressing these wave functions using Fourier series, in theory an infinite plane wave basis should be used, but in practice the series development is truncated at certain terms defined by the cut-off energy E_{cut}.

• We vary the energy E_{cut} from *200* to *900* for both of the compounds $CsBSe_3$ & $TlBSe_3$. For each value of E_{cut}, we calculate the total energy, and we plot the curve of variation of the energy E_{tot} as a function of E_{cut}.

All of the values in the BZ are taken by the wave vector k. In effect, the calculations must be performed using a finite set of k points, each of which is selected as low as achievable while a representative sample of the BZ is collected.

• After having set the value of cut-off energy, we proceed now to vary the number of *k* points, for the compound $TlBSe_3$, the *k* points were varied from (3x1x2) to (4x3x5), while for the compound $CsBSe_3$ they were varied from (2x1x2) to (7x3x6).

The following figure shows the convergence of total energy as a function of cut-off energy and the convergence of total energy as a function of Nk-points.

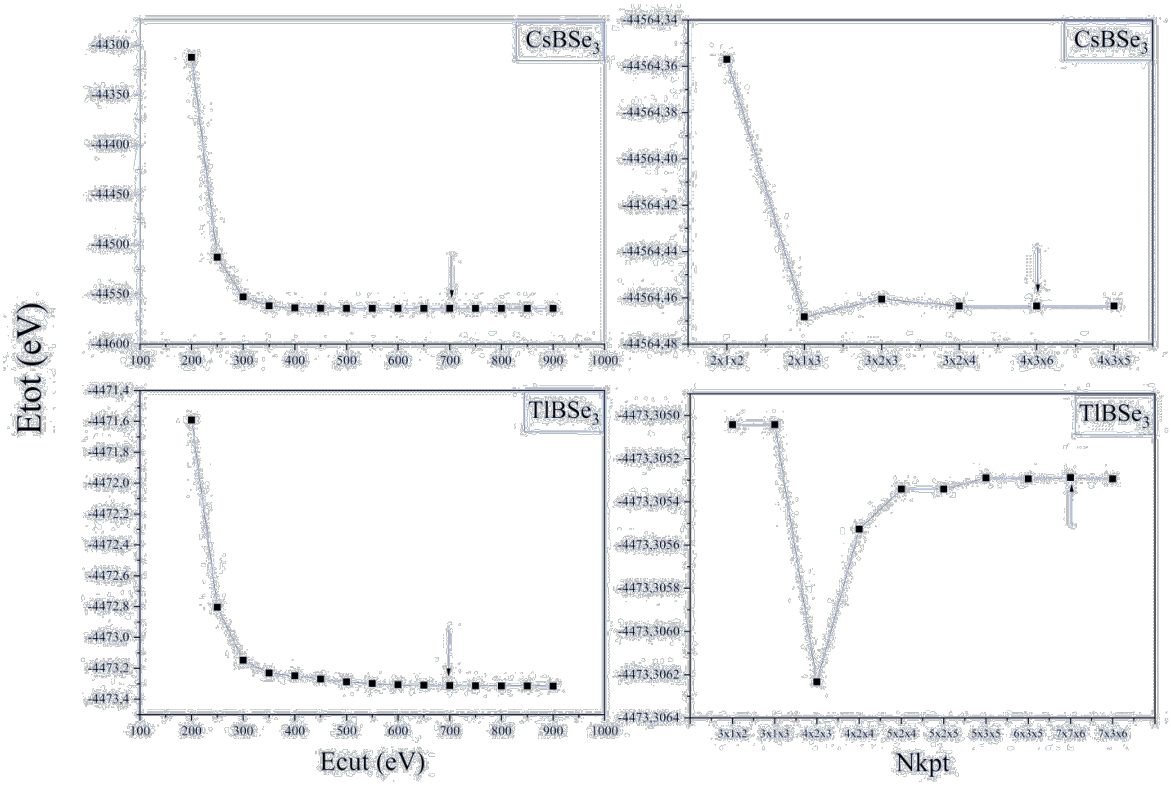

Fig III-1. Convergence of the total energy of $ABSe_3$ as a function of E_{cut} & Nk_{pt}.

As shown in ***Fig III-1.*** we took the values pointed with an arrow in order to calculate the optimization and the rest of the properties. *(For $CsBSe_3$ number of special points tokens was 24 while for $TlBSe_3$ 84).*

III-4. The structural properties of $ABSe_3$ materials

Before calculating the properties that we are looking for, we must first optimize the structure for a relaxed and more stable structure which corresponds to a minimum total energy. This consists in minimizing the forces known as Hellmann-Feynman [6, 7] forces exerted on each atom of the solid.

The structure of the studied $TlBSe_3$ and $CsBSe_3$ compounds is optimized by varying the lattice parameters (*a, b, c, β*) and the coordinates of the ions. The optimized structure represents a relaxed lattice (*i.e., minimize the components of the forces exerted on each atom*). The CASTEP code uses the Broyden-Fletcher-Goldfarb-Shanno (*BFGS*) [8] algorithm to vary all the structural parameters and find the equilibrium geometry.

In processing of optimization, the CASTEP code uses the following criterias:

- Tolerance with respect to energy: 5×10^{-6} eV/ion
- Tolerance with respect to maximum forces: 1×10^{-2} eV/Å
- Tolerance with respect to maximum stress: 2×10^{-2} GPa
- Tolerance with respect to the maximum displacement: 5×10^{-4} Å

• ***Fig III-2.*** Illustrates the monoclinic structure of the two compounds, for $TlBSe_3$ and $CsBSe_3$) described by $a \neq b \neq c$ and $\alpha = \gamma = 90°, \beta \neq 120°$.

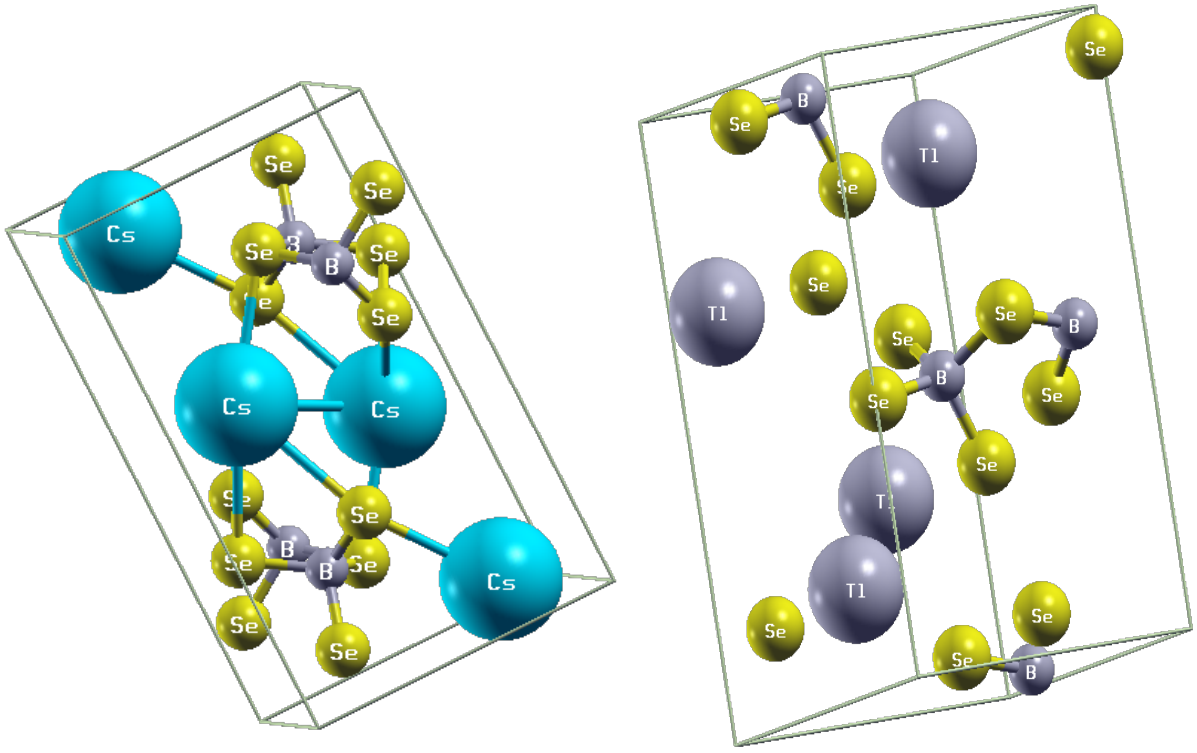

Fig III-2. The structure of the two compounds.

The most important step in ab-initio calculations is to determine the structural properties to gain more information about the properties of the material under study. Knowing this info later can give us access to other physical properties.

Table III-1. The structural parameters of ($ABSe_3$); Array parameter, density and volume [9].

Parameter		*$CsBSe_3$*			*$TlBSe_3$*
***a* (Å)**	a_{exp}	7.570(2)	$\Delta a/a$ (%)		6.166(2)
	a_{cal}	**7.831564**	**+3.46**	**+0.07**	**6.170083**
		7.74342676	*+2.29*	*+2.011*	*6.28997633*
***b* (Å)**	b_{exp}	12.791(4)	$\Delta b/b$ (%)		12.109(2)
	b_{cal}	**12.990769**	**+1.56**	**+2.69**	**12.435234**
		13.05376608	*+2.03*	*+9.69*	*10.93613605*
***c* (Å)**	c_{exp}	6.171(2)	$\Delta c/c$ (%)		7.031(2)
	c_{cal}	**6.205437**	**+0.56**	**+4.15**	**7.322962**
		6.29852291	*+2.07*	*-4.63*	*6.70560732*
β	β_{exp}	107.09(2) °	$\Delta\beta/\beta$ (%)		113.88(3) °
	β_{cal}	**105.66278**	**+1.33**	**-0.51**	**113.29915** °
		106.309841	*-0.73*	*-15.70*	*96.002688*
***V*(Å 3)**	V_{exp}	571.1(3)	$\Delta V/V$ (%)		480.1(2)
	V_{cal}	**607.886**	**+6.44**	**+7.49**	**516.046**
		611.240701	*+0.07*	*-4.45*	*458.7364402*
***ρ* (g/cm³)**	ρ_{exp}	4.426	$\Delta\rho/\rho$ (%)		6.255
	ρ_{cal}	**4.15863**	**-6.43**	**-6.98**	**5.81858**
		4.1692	*-5.80*	*+5.49*	*6.5988*

- **CASTEP**
- *CRYSTAL*

III-5. Electronic properties

The study of the electronic properties of a material takes a very important place because they allow us to understand the nature of the bonds that form between the different elements that make up this material and to specify its character (*insulator, semiconductor, conductor*). For the

electronic properties, we are interested in the study of the structure of the electronic energy bands and the density of states (*DOS*) and the charge density.

III-5-1. Band structure

The electronic band structure of solids reveals the eigenvalues associated with conduction and valence bands along specific directions in the *BZ* of a particular crystal structure.

One of the most important reasons for calculating the structure of electronic bands is to determine the gap energy which represents the difference between the values of the energies of the valence band and the conduction band.

we calculated the energy bands of $ABSe_3$ compounds (A= *Tl, Cs*) along the high symmetry directions of the first *BZ*, using the GGA-PBE approximation.

• ***Fig III-3.*** Illustrates the *BZ* related to the monoclinic structure for $ABSe_3$ compounds (A= *Tl, B*), with high symmetry k-points, used for calculation of band structure.

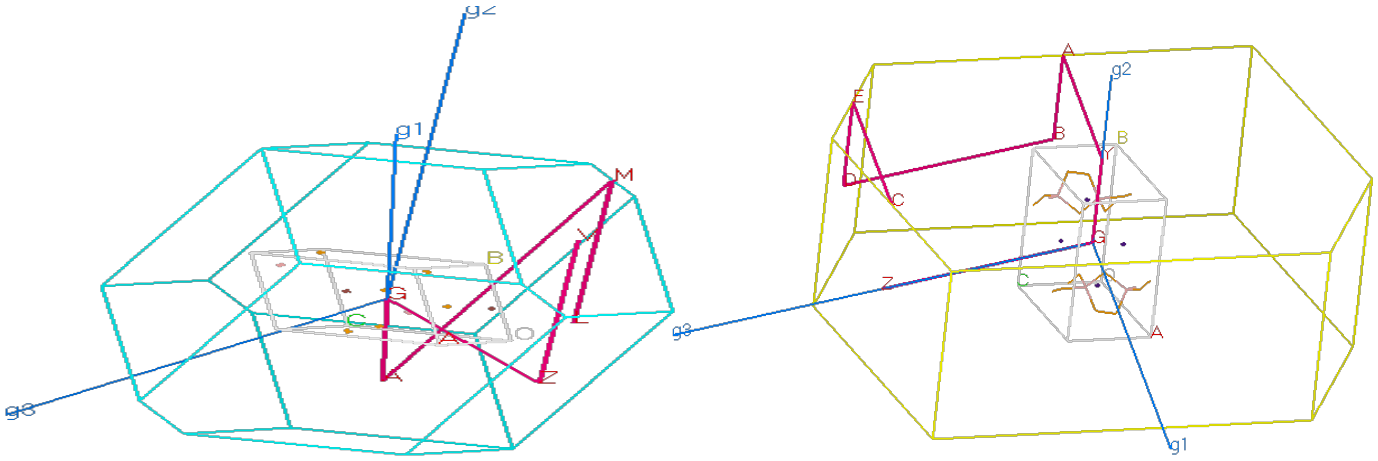

• ***Fig III-3.*** The *BZ* related to the monoclinic structure for *$CsBSe_3$ (left)* and *$TlBSe_3$ (right)*.

The six high symmetry *k* points of the *BZ* for the monoclinic network are the following coordinates:

• ***$TlBSe_3$:*** *L(-0.5, 0, -0.5); M(-0.5, 0.5, -0.5); A(-0.5, 0, 0); G(0, 0, 0); Z(0, -0.5, -0.5); V(0, 0, -0.5).*

• ***$CsBSe_3$:*** Z(0, 0, 0.5) ; G(0, 0, 0) ; Y(0, 0.5, 0) ; A(-0.5, 0.5, 0) ; B(-0.5, 0, 0) ; D(-0.5, 0, 0.5) ; *E(-0.5 ,0.5, 0.5) , C(0, 0.5, 0.5)*

• ***Fig III-4.*** represent the electronic band structures according to the high symmetry directions of the *1st BZ* for *$ABSe_3$* compounds, calculated by the *GGA-PBE* approximation.

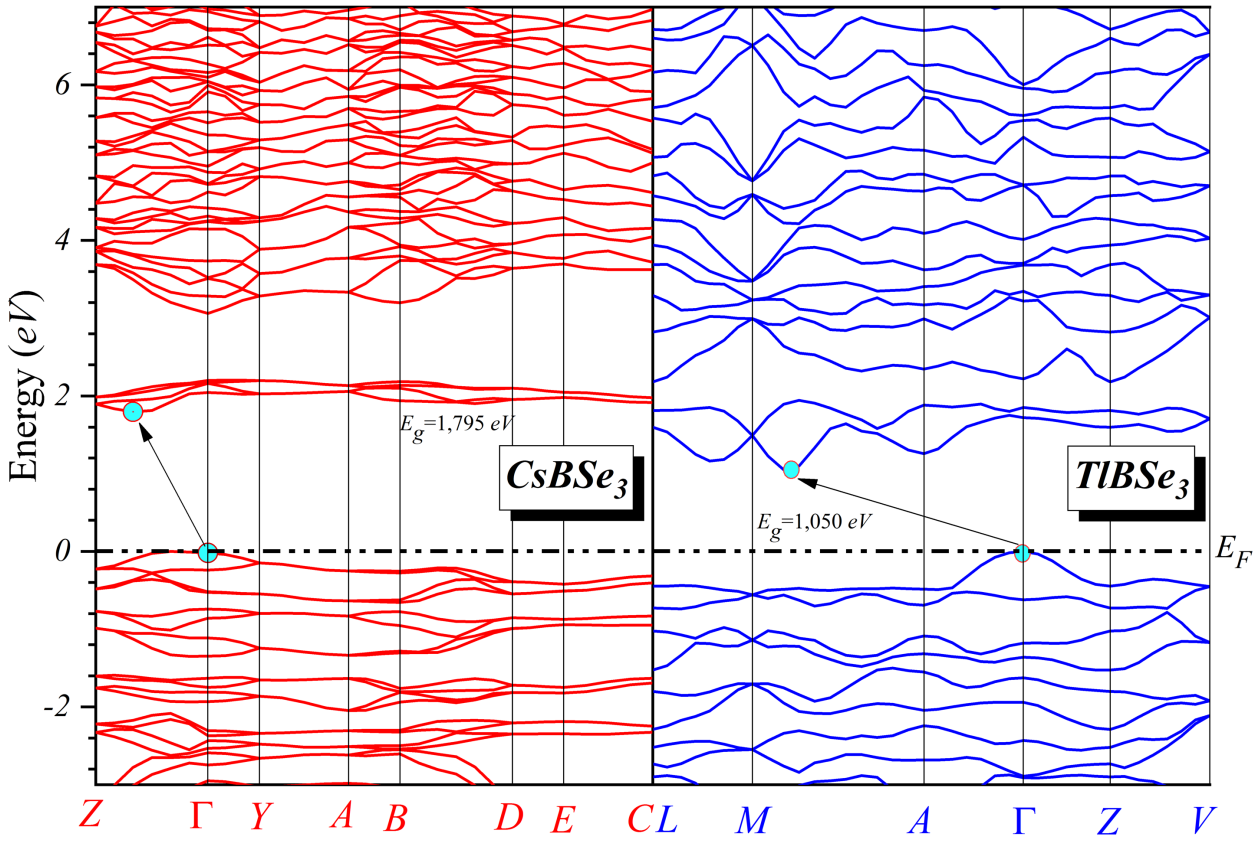

Fig III-4. The electronic band structure of the *$ABSe_3$* compounds.

The diagrams in ***Fig III-4*** show that the two materials are indirect gap semiconductors. Indeed, the maximum of the valence band (*BV*) is located at the point Γ for *$TlBSe_3$* & *$CsBSe_3$*, while the minimum of the conduction band (*BC*) is found at the point between *M* and *A* for *$TlBSe_3$*, and between *Z* and Γ for *$CsBSe_3$*, which gives us an indirect gap demonstrated in ***Table III-2***. However, knowing the trend general *GGA* to underestimate this value [10], the real values must be higher.

Table III-2. Numerical comparison between our calculated gap and other calculus [11].

Material	*Gap value*	
$CsBSe_3$	E_g = 1.7859 eV indirect	E_g = 1.9780 eV direct
	Our calculi: 1.7850 eV	
$TlBSe_3$	E_g = 0.8410 eV indirect	E_g = 1.4700 eV direct
	Our calculi: 1.0500 eV	

III-5-2. The density of state

The electronic density of state (*DOS*) gives information on the occupation of the electronic bands of a material [12]. We calculated the density of states of $ABSe_3$ compounds (A= *Tl, Cs*), using the *GGA-PBE* approximation.

The calculated total and partial densities of states are presented in ***Fig III-5*** and ***Fig III-6***. The Fermi level beings to be taken as the origin of the energies.

• For the compound $TlBSe_3$ the first valence region is located at approximately (-16, -10), this region is essentially dominated by the *s* states of *Se* and the *d* states of *Tl* with a small contribution from the *s* and *p* states of the *B* atom. The second region between (-7.5, 0), which is dominated by the *p* states of *Se* with a weak contribution of *s* and *p* of *B*. The last region (1.05, 16), is the conduction band, it is dominated by the *s* and *p* states of *Se* and the *p* states of *Tl* with low *s* and *p* contribution from *B*.

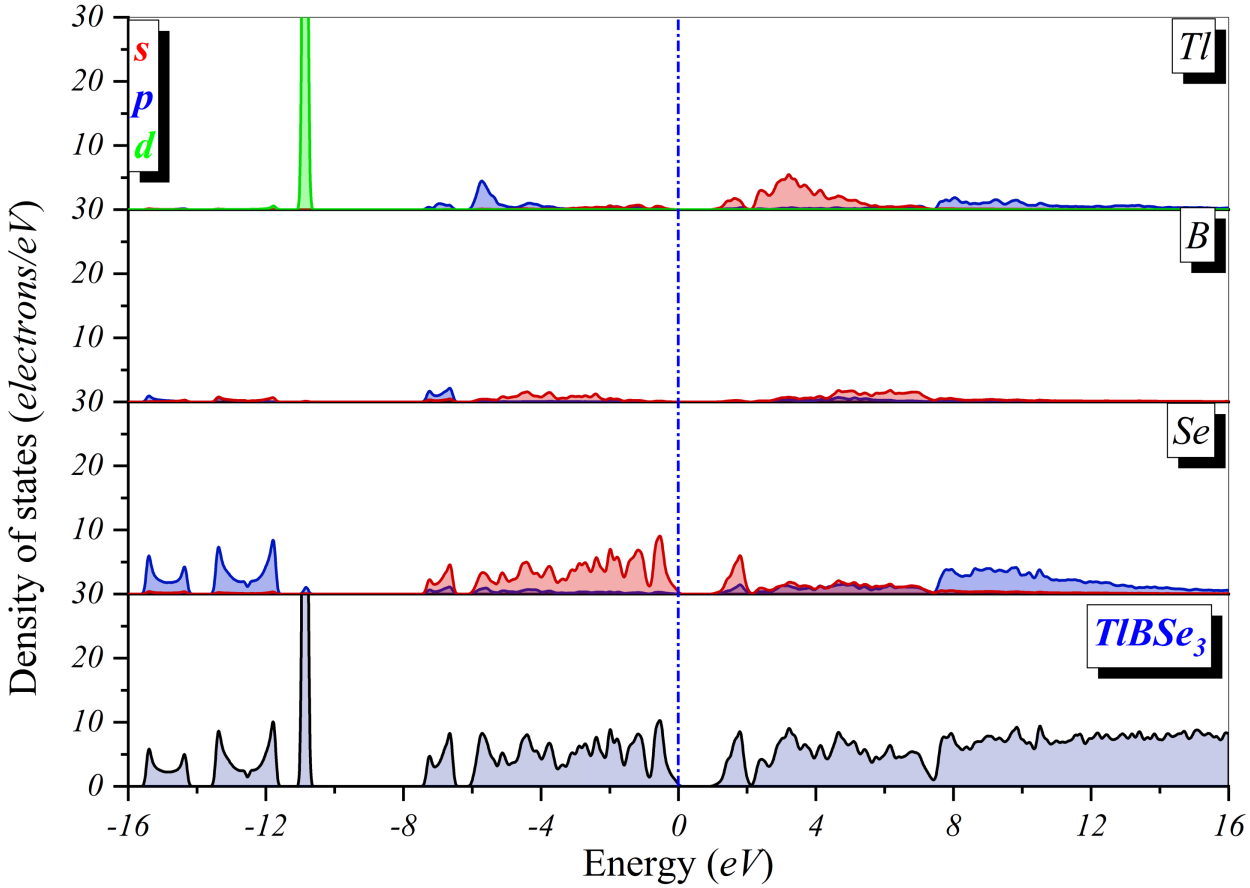

Fig III-5. Distribution of the electronic density of states in $TlBSe_3$.

• For the compound $CsBSe_3$ the first region of valence is located between (-16, -11) and it is dominated by the *s* states of *Se* with a weak contribution of the *s* and *p* states of *B*. The second region at about (-9, 0), is dominated by the *p* states of *Cs* and the *p* states of *Se* with a weak contribution of *s* and *p* of *B*. The last region in the conduction band (1.7, 16), is dominated by the *s* states of *Se* and the *p* states of *Cs* with a weak contribution of the *p* states of *B*.

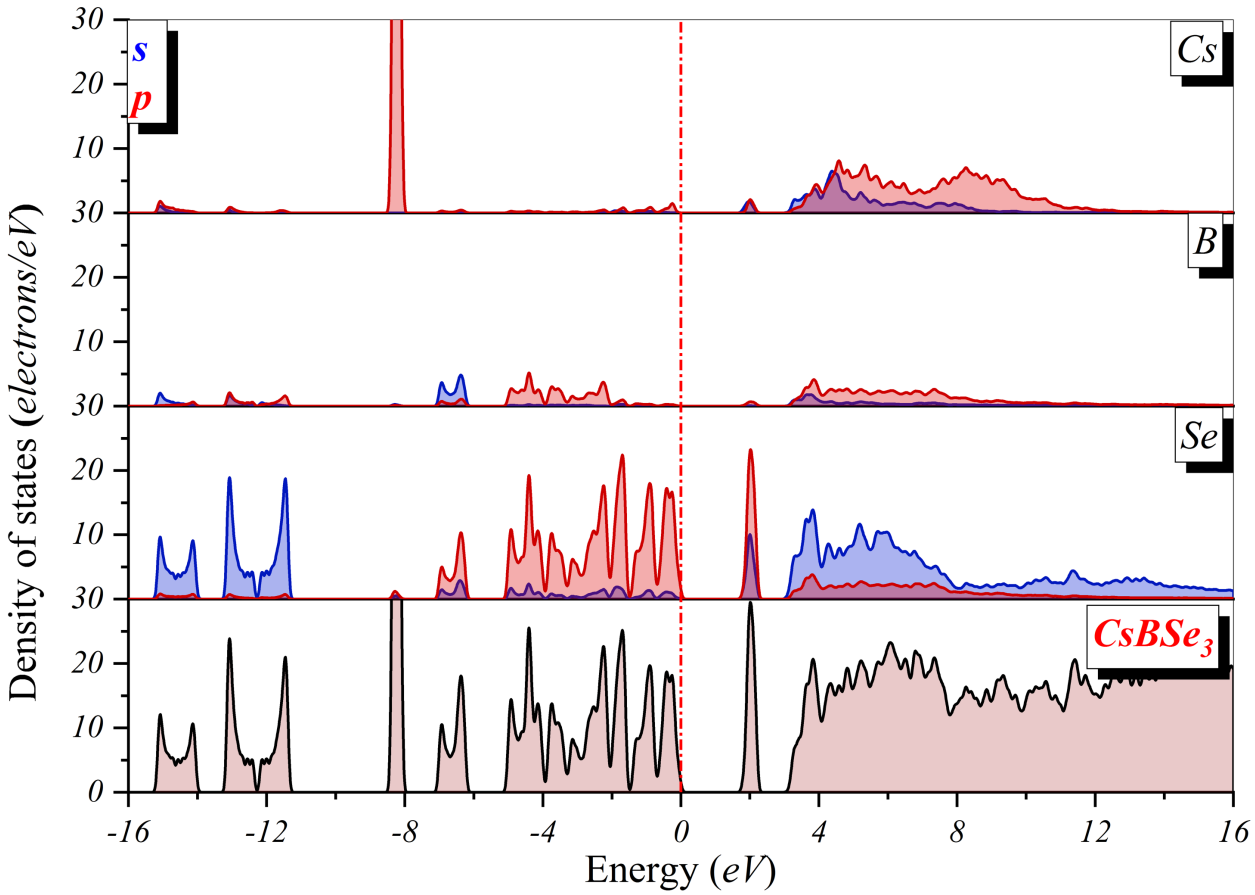

Fig III-6. Distribution of the electronic density of states in $CsBSe_3$.

III-5-3. Atomic Populations (Mulliken)

The charge density distribution is an important property of solids as it provides a good description of chemical properties. Chemical bonding results from the distribution of electronic charge between atoms.

Determining the nature and the behavior in a given solid requires the study of the electronic charge density, which plays an important role in determining all the chemical and physical properties of a compound.

The ionic character of a material can be linked to the transfer of charge between the cations and the anions which constitute it. For this reason, in order to explore the bonds of the two $ABSe_3$ materials (A = *Cs, Tl*), we calculated the charge transferred between the cations and the anions of the two compounds based on the Mulliken population analysis.

The calculation results ; partial charge of the orbitals, total charge for each atom and the charge transferred between the cations and the anions, they are gathered in ***Table III-3***.

Table III-3. Partial and total loads and transferred loads for $ABSe_3$ from the Mulliken population analysis.

$ABSe_3$		s(*e*)	p(*e*)	d(*e*)	Total (*e*)	charge (*e*)
$TlBSe_3$	*Tl*	1.87	0.70	10.00	12.57	0.43
	B	1.11	2.26	0.00	3.37	-0.37
	Se	1.82	4.17	0.00	5.99	0.01
$CsBSe_3$	*Cs*	2.10	6.20	0.00	8.30	0.70
	B	1.11	2.25	0.00	3.36	-0.36
	Se	1.81	4.29	0.00	6.10	-0.10

• This table shows that the charges transfer *Cs* to *B* and *Se* for the $CsBSe_3$ material, such that each *Cs* atom loses 0.70 *e,* while for the $TlBSe_3$ material, the charges transfer from *Tl* to *B*, such that *Tl* loses 0.43 *e* and *B* receives 0.37 *e.*

Table III-4. Mulliken population of atomic bonds in our $ABSe_3$ materials.

$ABSe_3$	Bond	Population	Length (Å)
$TlBSe_3$	*B -- Se*	0.57	2.03323
	Se -- Tl	-1.47	3.38154
	B -- Tl	-0.21	4.09742
$CsBSe_3$	*B -- Se*	0.38	2.03115
	Se -- Se	-2.45	2.35023
	Se -- Cs	-0.63	3.68036
	B -- Cs	0.26	4.56202

• According to ***Table III-4***, the population of *B -- Se* and *B -- Cs* bonds indicate the weak ionic character of these bonds in the $CsBSe_3$ material, the negative populations of *Se -- Cs* and *Se -- Se* bonds indicate an anti-binder between these two ions. For the $TlBSe_3$ material, the *B -- Se* bond indicates the weak covalent character, while the interaction between *Se* and *Tl* is an anti-bonder.

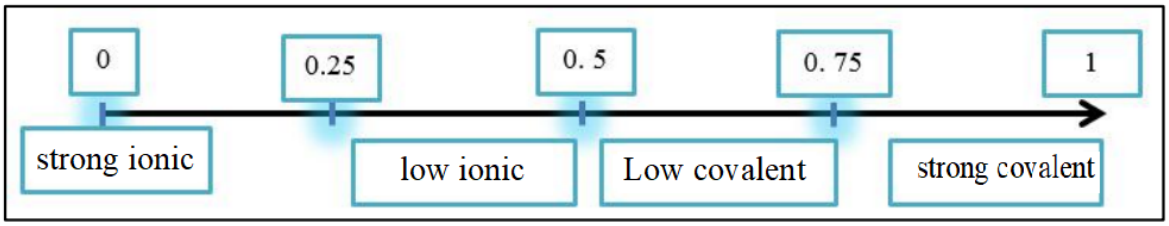

Fig III-7. Classification of bonds according to their electronic population.

III-6. Optical properties

When an electromagnetic wave of sufficient power shines on a material, it induces transitions of electrons between occupied states (*below* E_F) and unoccupied states (*above* E_F). It is clear that the study of these transitions should provide some understanding of the electronic properties of materials such as the structure of energy bands.

Spectra of reflectivity, absorption, refractive index, extinction coefficient and dielectric function describing the optical response of our materials $ABSe_3$ were calculated over a wide spectral range for three polarizations of the incident wave. In this section, the results are from a purely predictive study performed in the GGA-PBE approximation with a denser sampling grid of *k-points* 4×3×6 ($CsBSe_3$) and 7×7×6 ($TlBSe_3$), for maximum separation of 0.05 $Å^{-1}$ along the main [1 0 0] axis of the reciprocal lattice and corresponding to 50 *k-points* ($CsBSe_3$) and 160 *k-points* ($TlBSe_3$), will be presented in this part for the polycrystal.

III-6-1. The dielectric function

In order to check the optical property of our studied materials we have engaged in a calculation of a complex dielectric function $\varepsilon(\omega)$ which describes the optical response of a material, determined by the electronic transitions between conduction bands and valence bands. It involves a real part $\varepsilon_1(\omega)$ and another imaginary $\varepsilon_2(\omega)$. $\varepsilon_2(\omega)$describes the absorption of electromagnetic radiation and $\varepsilon_1(\omega)$ describes the dispersion of this radiation in the material. As the dielectric

function describes a causal relationship, both real and imaginary parts are related to each other. Thus $\varepsilon_1(\omega)$ is calculated in a simple way using a Kramers-Kornig transformation (*see Chapter II*).

It is calculated by evaluating the elements in representation of the impulse, given by the following relation [13]:

$$\varepsilon = \varepsilon_1 + i\varepsilon_2 \qquad III-(01)$$

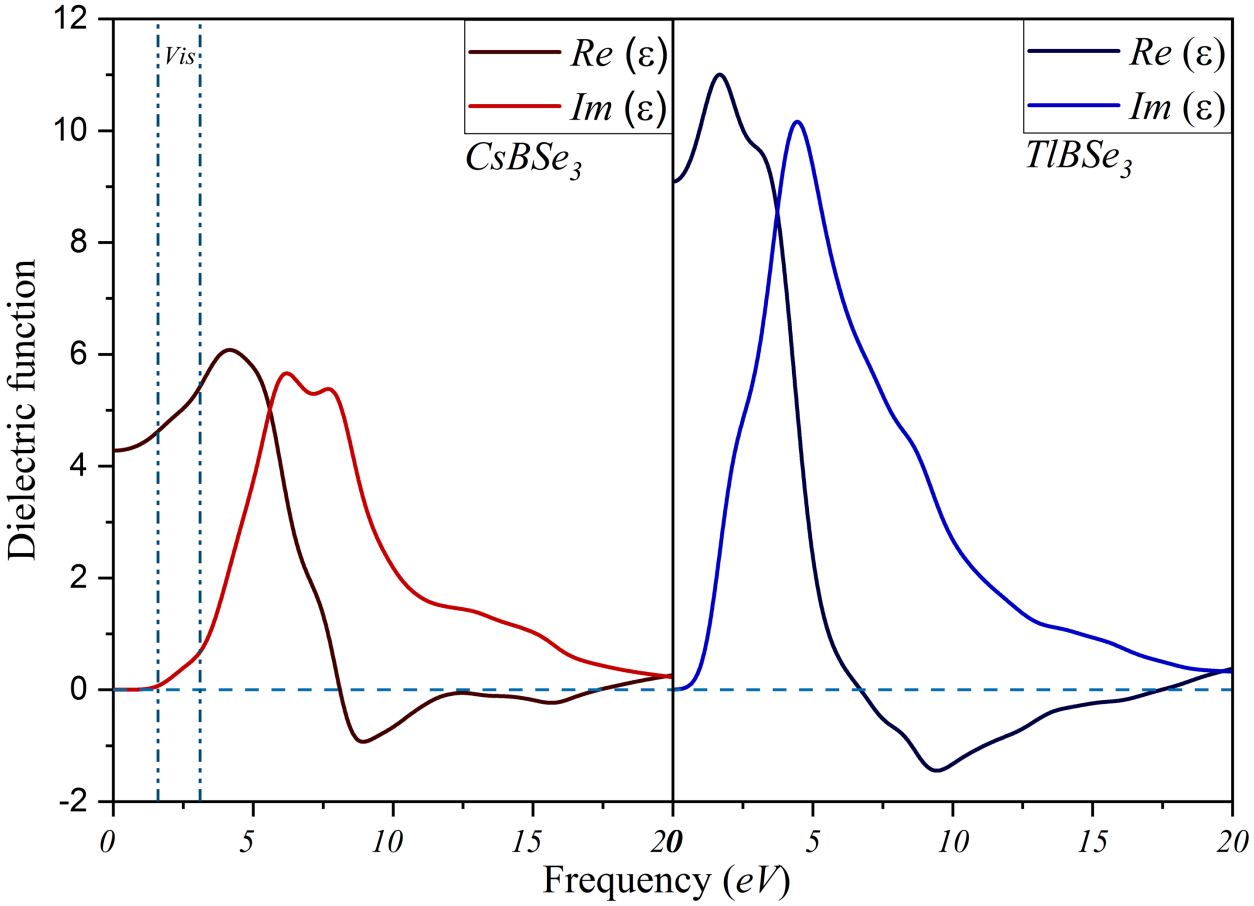

Fig III-8. The spectral dependence of the real and imaginary parts of the dielectric function.

The real part is determined from the imaginary part $\varepsilon_2(\omega)$, they are linked by the *Kronig-Kramers* relation [14] (*see Chapter II*).

The imaginary part is given by the following relation [15]:

$$\varepsilon_2(\omega) = \frac{4\pi e^2}{m^2\omega^2}\sum_{\varphi_i\varphi_f}\int\frac{2d^3\boldsymbol{k}}{(2\pi)^3}\left|\langle\varphi_{fk}|e.p|\varphi_{ik}\rangle\right|^2 f_{ik}(1-f_{fk})\delta\left[E_f(\omega)-E_i(\omega)-\hbar\omega\right] \qquad III-(02)$$

With: e is the electron charge and m is its mass.

φ_{ik} is the initial energy-filled state E_i.

φ_{fk} is the empty final state of energy E_f.

The imaginary part $\varepsilon_2(\omega)$ of the dielectric constant depends on the electronic transition at the origin of the absorption. We can derive the direct interbond transitions from the identification with the energy band structure. It [16] describes the absorption of the electromagnetic radiation, and can be expressed in the dipole approximation by the matrix element of transitions between the occupied valence bands and the unoccupied conduction band, while the real part of the electric function $\varepsilon_1(\omega)$ describes the incident radiation in the medium, and it can be derived from $\varepsilon_2(\omega)$ by Kramers-Kronig transformation [17, 18]. we have also calculated other optical parameters such as the reflectivity coefficient $R(\varepsilon)$, the absorption coefficient $\alpha(\varepsilon)$ and optical conductivity $\sigma(\varepsilon)$. All previous optical parameters, besides the real and imaginary parts are displayed next.

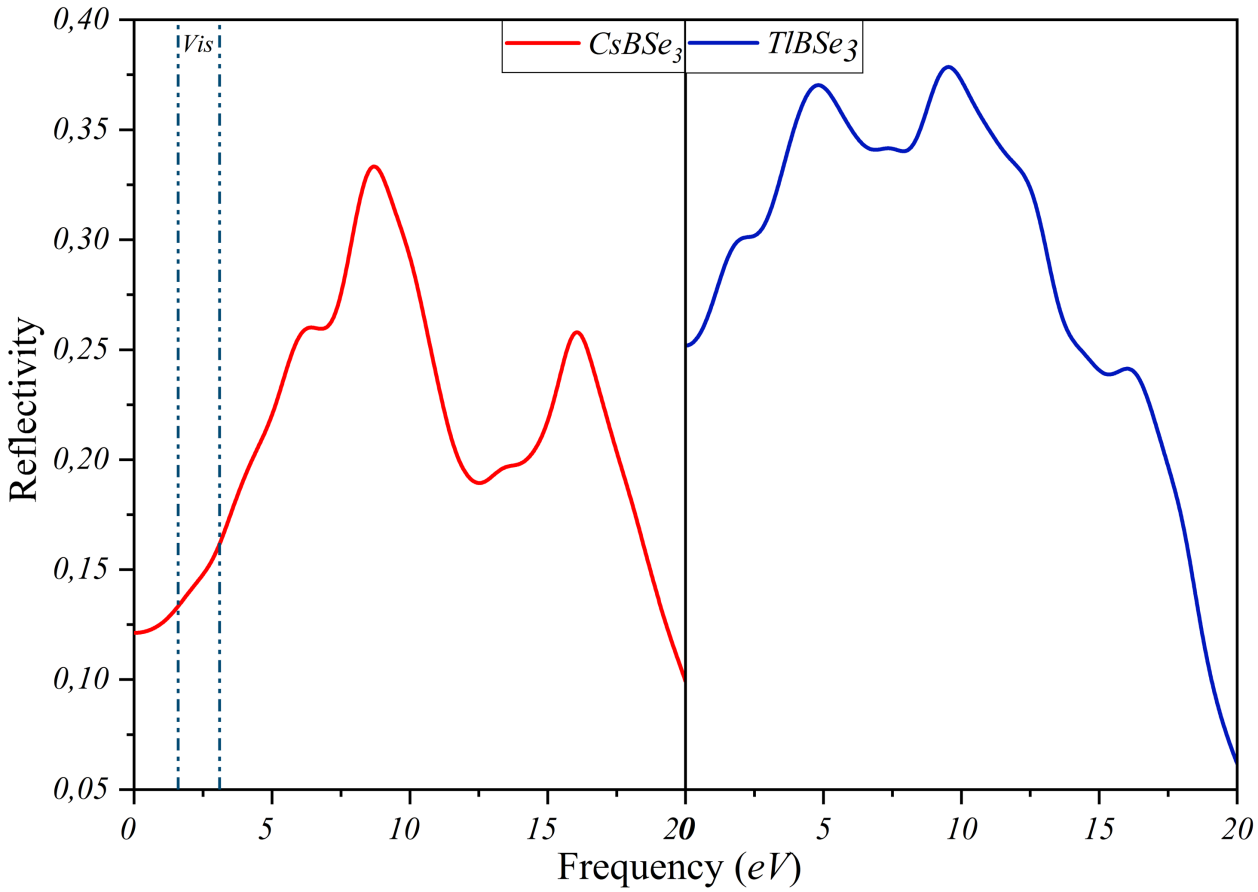

Fig III-9. $R(\varepsilon)$ as a function of the frequency.

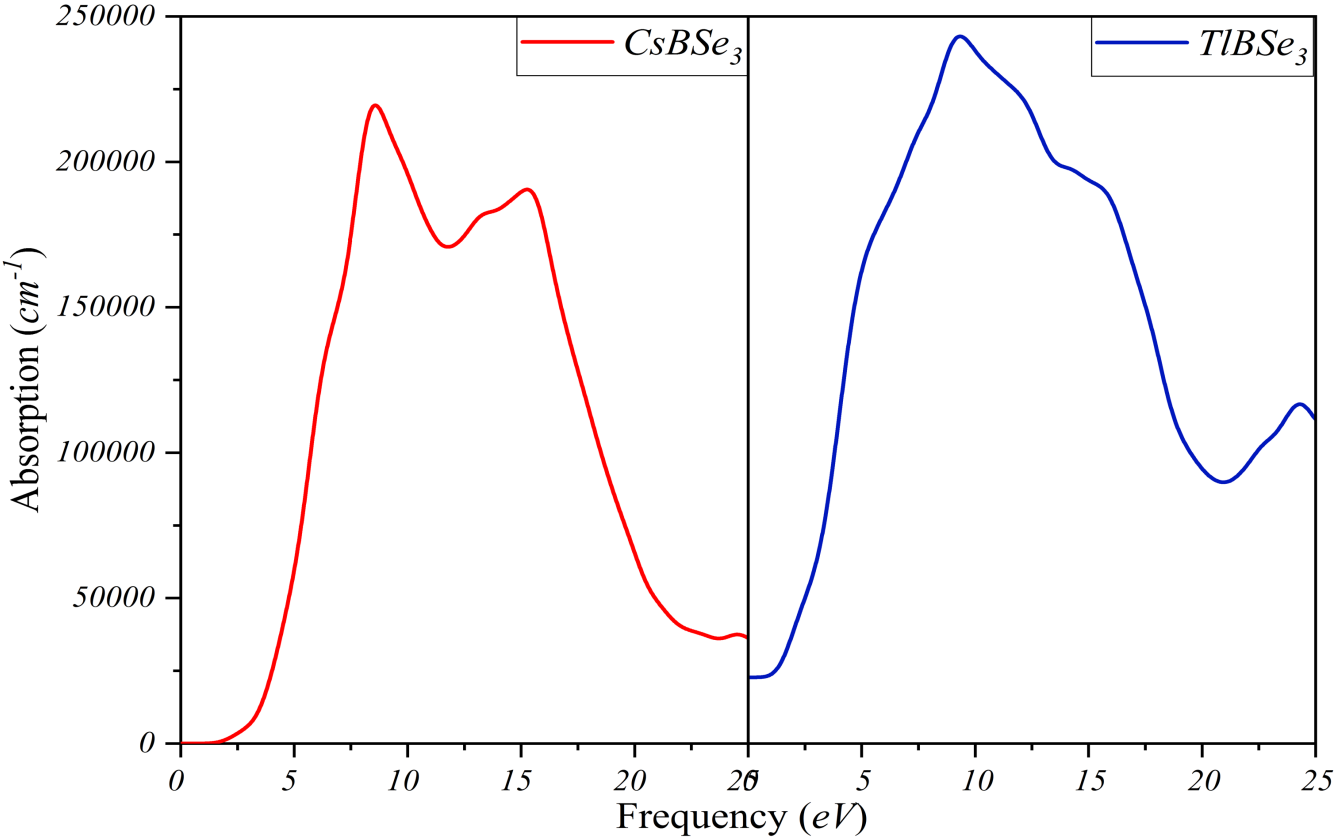

Fig III-10. *α(ε)* as a function of the frequency.

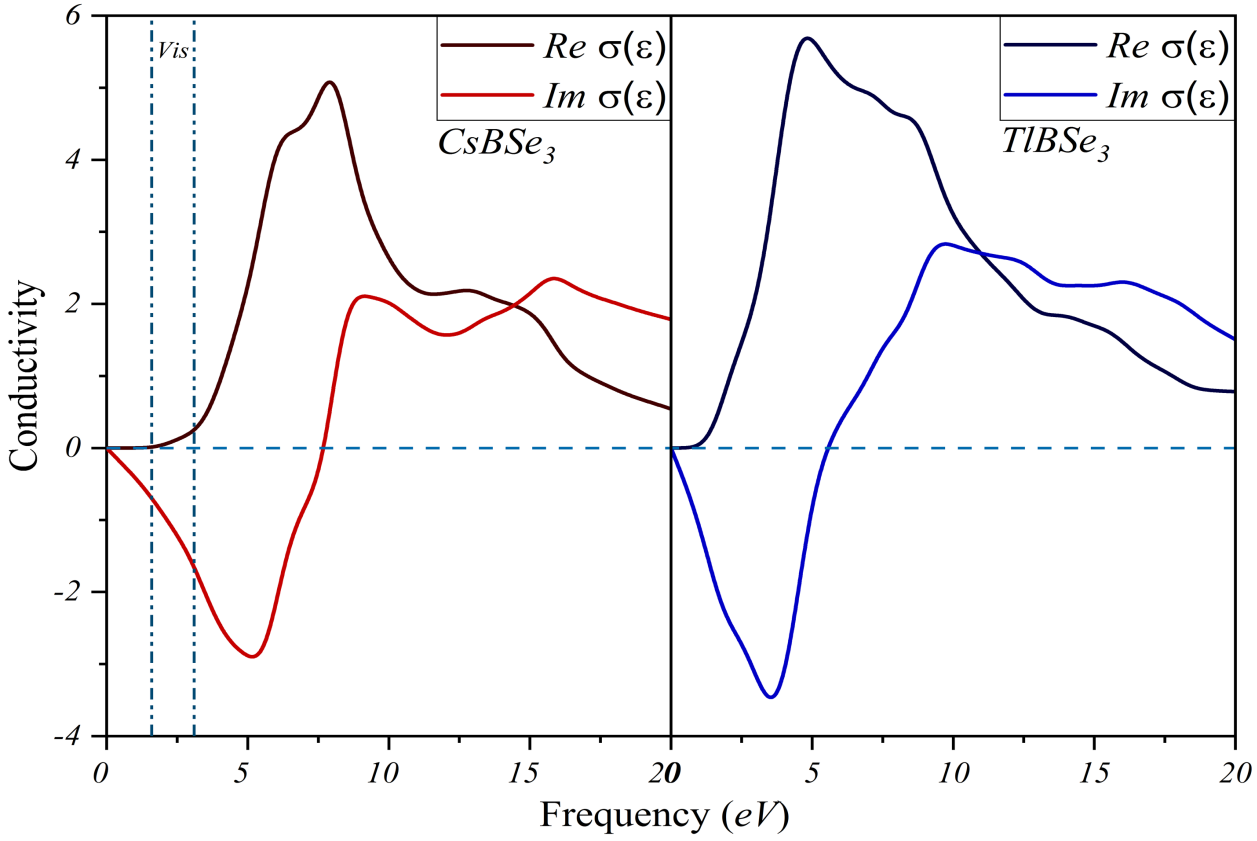

Fig III-11. *σ(ε)* as a function of the frequency.

It can be seen from the previous figures that the inexistence of the imaginary part at zero energy (*no absorption of light*) then starts rising after, leading to an energetic gap for both materials $CsBSe_3$ & $TlBSe_3$ which confirming the semiconducting behavior.

The optical conductivity $\sigma(\varepsilon)$ is deduced from the dielectric function which can be obtained from [19]. The optical conductivity begins rising to a maximum value.

The reflectivity of light $R(\varepsilon)$, which characterizes the part of energy reflected at the interface of the solid is also an important optical parameter when studying semiconducting materials for solar cell applications. In our case the reflectivity of $CsBSe_3$ & $TlBSe_3$ reach 35%, also we note that the maximal reflection occurs when ε_1 go towards the negative values.

For the absorption coefficient it can be said that from 0 eV to the upper infrared limit, α is zero, which means that our materials are transparent, from this point, α shows a very intense absorption, and it increases due to phonon excitations. This clearly indicates that our materials are active in this spectral range.

III-7. Elastic properties

The elastic properties of a solid are completely described by the tensor of the elastic constants C_{ij}. The elastic constants C_{ij} determine the response of a material to external forces (*stresses*), they play a very important role in the mechanical resistance of the material, in particular, for homogeneous solids, they also provide us with information on the character of the bonds between the adjacent atomic planes, as they can be a source of information on the anisotropy in the material and finally the mechanical stability of the structure. In *CRYSTAL*, the tensor of the C_{ij} is calculated by the strain-stress method, in which, a strain is applied to the crystal and then, in a geometry optimization process where only the atomic positions are relaxed, the free energy of the deformation and the stress associated with it is calculated according to equations $(03) - (05)$. This allows by an adequate choice of the deformation (*respecting the space group*) to deduce the tensor of C_{ij} [20].

$$\frac{\Delta E}{V_0} = \frac{1}{2}\sum_{i=1}^{6}\sum_{j=1}^{6} C_{ij}e_i e_j \qquad III-(03)$$

$$\Delta E = E(V,\sigma) - E(V_0,0) \qquad III-(04)$$

$$\sigma_i = \frac{1}{V_0}\frac{\partial E}{\partial e_i} = \sum_{j=1}^{6} C_{ij}e_j \qquad III-(05)$$

In this work, we were able to determine these constants by imposing a series of deformations respecting the monoclinic symmetry of the systems studied, then the resulting stress is calculated after relaxation of the atomic positions. The preselenborates $ABSe_3$ which crystallizes in the monoclinic system have the constants C_{11} C_{12} …… C_{66} *(see chapter II).* The values predicted by our calculations are shown in ***Table III-5.***

Our results show that:

- The mechanical stability conditions (*Born criteria*) are all satisfied (*see the stability criteria in the chapter II*), both materials are therefore mechanically stable.
- The values of C_{11} and C_{22} and C_{33} are relatively high, so the two $ABSe_3$ materials resist well to compression under the action of uniaxial stress along the three directions *x, y* and *z.*

Table III-5. The C_{ij} values (*in GPa*) calculated by GGA-PBE for the two $ABSe_3$ compounds.

Materials	$TlBSe_3$	$CsBSe_3$
C_{11}	114.40828704	26.32483211
C_{12}	84.74695509	11.57753375
C_{13}	24.52980774	7.07669017
C_{22}	122.582	32.419
C_{23}	19.51325906	8.66748623
C_{33}	93.82046634	55.67743337
C_{16}	-0.00000000	-0.00000000
C_{26}	0.00000000	-0.00000000
C_{36}	-0.00000000	0.00000000
C_{44}	20.03382652	7.97277177
C_{45}	0.00066134	-0.09645464
C_{55}	7.47401372	5.05803863
C_{66}	40.33982454	10.36595675

III-7-1. The moduli of elasticity

The calculation of the moduli of elasticity makes it possible to calculate other quantities related to these (*Mechanical Quantities*) such as the modulus of compressibility, the modulus of Yong, shear and coefficient of poison are calculated from the elastic constants.

The following table presents the compressibility modulus, Young's modulus (E), shear modulus (G) and Poisson's ratio (ν) for our compounds in the GGA-PBE approximation.

There are no theoretical or experimental values of G and B for the two compounds. The values of E, and B/G are close to those calculated theoretically.

Table III-6. Elastic modulus of our materials.

Compound	G_V	G_R	G	B_V	B_R	B	E	ν	B/G
$TlBSe_3$	27.06	13.16	20.11	65.31	58.61	61.96	54.44	0.354	3.08
$CsBSe_3$	10.486	7.33	8.908	18.79	16.50	17.645	22.88	0.284	1.98

- The value of B (*BULK MODULUS*) of the compound $TlBSe_3$ is larger than that of $CsBSe_3$. This means that the $TlBSe_3$ material is more resistant to a change in volume under the action of hydrostatic pressure.
- Young's modulus E and shear modulus G of $TlBSe_3$ is large than $CsBSe_3$, so $TlBSe_3$ material is more tensile and shear resistant.
- For the classification of compounds as fragile or ductile material, the B/G ratio was calculated, with the critical value which separates ductile/fragile behavior equal to 1.75 (fragile<1.75<ductile), so we note that the values of the B/G ratio of the compounds $TlBSe_3$, $CsBSe_3$ are respectively 3.08 and 1.98 for GGA-PBE then these materials are ductile.

III-7-2. Debye temperature

We calculated the Debye temperature for the $ABSe_3$ materials in the GGA-PBE approximation from the average speed of sound v_m calculated from the elastic moduli (see chapter I). The results obtained are distributed in ***Table III-8***.

Table III-7. Calculation of the longitudinal velocity v_l, the transverse velocity v_t , the average velocity v_m , and the Debye temperature in the GGA-PBE approximation.

Materials	ρ	v_l	v_t	v_m	θ_D
$TlBSe_3$	6.59889	3668	1746	2359	248
$CsBSe_3$	4.1692	2661	1462	1916	183

III-7-3. Anisotropy of elastic behaviour

Many materials' deformation behaviour is orientation-dependent. That implies, if a sample were removed from a material and born in a different direction, the stress-strain response would be different. Hypothetically, a material's degree of anisotropy can be described in many ways:

By the universal anisotropy index, a zero value indicates a perfect isotropic elastic response, while a higher value indicates some degree of anisotropy, the elastic response of both materials is strongly anisotropic. In addition, *TlBSe₃* exhibits the greatest degree of elastic anisotropy.

- By the percentage of anisotropy in compression and in shear, a zero value indicates an isotropic behavior of the modulus of elasticity considered, while a value different from zero indicates a certain degree of anisotropy.
- It is well recognized that shear anisotropy is intimately linked to the movement of dislocations and to the creation and propagation of cracks. The shear anisotropy in the main planes can be characterized by the anisotropy factors, a value close to unity indicates isotropic behavior in the considered plane, while any deviation from unity indicates some degree of anisotropy .
- The studies mentioned above are insufficient to describe the anisotropy of the elastic behavior of a crystal. Another useful and more convenient way to quantify the elastic anisotropy consists in studying the directional dependence of the different moduli of elasticity such as the shear modulus and the compressibility modulus, which are also the two most used parameters for the description of the elastic behavior of materials. On a *3D* surface, the modulus of the position vector of a point represents the value of the elastic quantity measured in the direction of this vector.

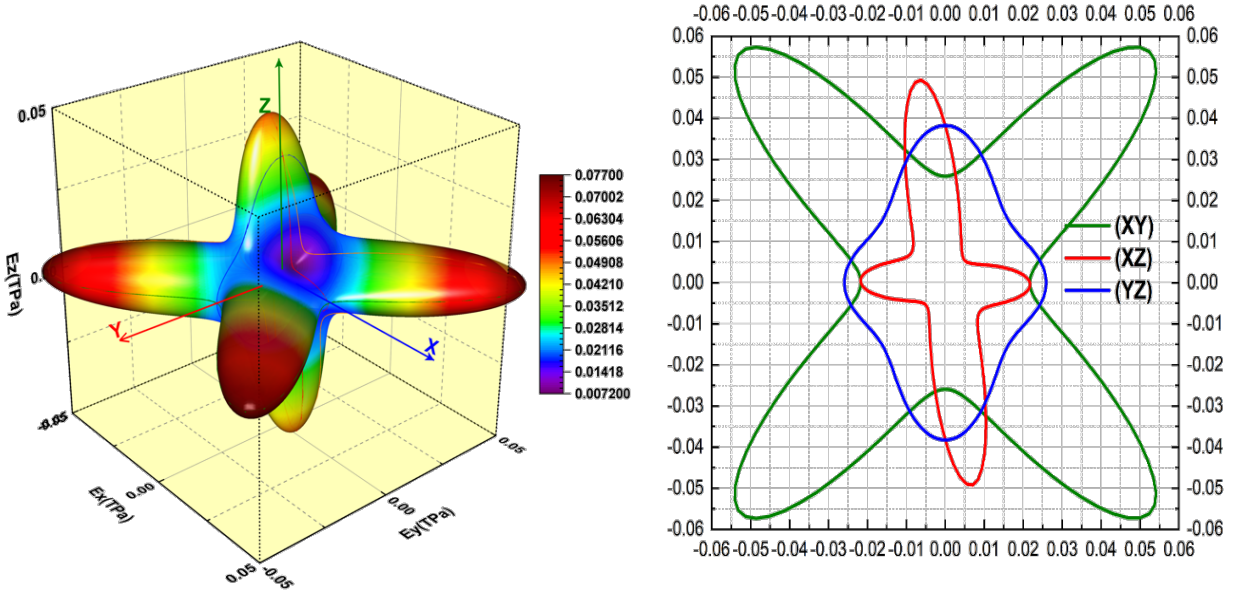

Fig III-12. *3D* representation of the dependence of the modulus of compressibility (*left*) and the intersections of the surface with the planes (*xy*), (*xz*), (*yz*) (*right*) for *CsBSe₃* compound.

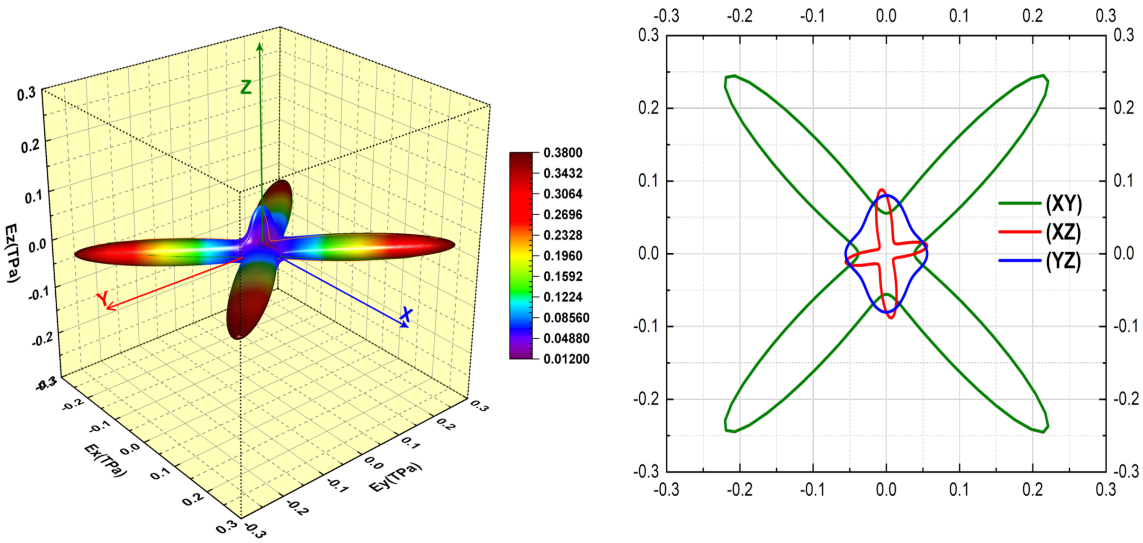

Fig III-13. *3D* representation of the dependence of the modulus of compressibility (*left*) and the intersections of the surface with the planes (*xy*), (*xz*), (*yz*) (*right*) for $TlBSe_3$ compound.

Conclusion

This work is a contribution to the study of the structural, elastic, electronic and optical properties of perselenoborates $CsBSe_3$ & $TlBSe_3$. Relevant bibliographic research has allowed us to see that very little is known about the fundamental physical properties of these materials. In response to the lack of studies on this subject, we set ourselves the objective of establishing a credible knowledge base from a series of ab-initio simulations based on the density functional theory by means of the approximation of the generalized guardian GGA-PBE.

III. References

[1]. Segall, M., et al., First-principles simulation: ideas, illustrations and the CASTEP code. Journal of Physics: Condensed Matter, 2002. **14**(11): p. 2717.

[2]. D. Vanderbilt, *Phys. Rev. B*. 1990, 41, 7892-7895.

[3]. R. Dovesi, A. Erba, R. Orlando, C.M. Zicovich-Wilson, B. Civalleri, L. Maschio, M. Rérat, S. Casassa, J. Baima, S. Salustro, B. Kirtman, Quantum-mechanical condensed matter simulations with CRYSTAL, Wiley Interdiscip. Rev. Comput. Mol. Sci. 8 (2018) 1–36. doi:10.1002/wcms.1360.

[4]. J. P. Perdew, K. Burke and M. Ernzerhof, *Phys. Rev. Lett*. 1996, 77 (18), 3865.

[5]. H .J. Monkhorst and J .D. Pack, *Phys. Rev. B*. 1976, 13 (12), 5188.

[6]. R. Feynman, *Phys. Rev*. 1939, 56, 340.

[7]. H. Hellmann. Franz Deuticke, Leipzig, 1937.

[8]. Head, J. D., & Zerner, M. C. (1985). A Broyden–Fletcher–Goldfarb–Shanno optimization procedure for molecular geometries. *Chemical physics letters*, *122*(3), 264-270.

[9]. Syntheses, Crystal Structures, and Properties of the Three Novel Perselenoborates RbBSe3, CsBSe3, and TlBSe3 with Polymeric Chain Anions, Arno Lindemann, Journal of Solid-State Chemistry 157, 206_212 (2001).

[10]. R.W. Godby, M. Schluter and L. Sham, *Phys. Rev. B.* 1987, 36, 6497.

[11]. discover.materialscloud.org

[12]. CHIHI. Tayeb: these de doctorat, UNIVERSITE FERHAT ABBAS-SETIF.

[13]. Hosseini, S., T. Movlarooy, and A. Kompany, *First-principles study of the optical properties of PbTiO 3.* The European Physical Journal B-Condensed Matter and Complex Systems, 2005. **46**(4): p. 463-469.

[14]. Lucarini, V., Saarinen, J. J., Peiponen, K. E., & Vartiainen, E. M. (2005). *Kramers-Kronig relations in optical materials research* (Vol. 110). Springer Science & Business Media.

[15]. Smith, N. V., & Woodruff, D. P. (1986). Inverse photoemission from metal surfaces. *Progress in surface science*, *21*(4), 295-370.

[16]. H. Ehrenreich, M.L. Cohen, Phys. Rev. 115 (1959) 786.

[17]. H.A. Kramers, Nature 113 (2845) (1924) 673e674.

[18]. De L.R. Kronig, J. Opt. Soc. Am. 12 (6) (1926) 547e557.

[19]. H.G. Tompkins, E.A. Irene, Handbook of Ellipsometry. William Andrew, Norwich, NY, 2005.

[20]. Caro, M.A., S. Schulz, and E.P. O'Reilly, Comparison of stress and total energy methods for calculation of elastic properties of semiconductors. Journal of Physics: Condensed Matter, 2012. **25**(2): p. 025803.

→ *"A person who never made a mistake never tried anything new."*

– Albert Einstein–

GENERAL CONCLUSION • • •

CONCLUSION

By a *DFT* approach, we studied the structural, electronic, elastic, and optical properties of semiconductors belonging to the family of perselenoborate $ABSe_3$ We have adopted in this study the pseudo-potential technique coupled with the plane-wave method implemented in the *CASTEP* code. For the treatment of the exchange and correlation term, we used two approaches.

The first one is based on the generalized gradient approximation *GGA* parameterized by Perdew-Burk-Ernzerhof. To give a better estimate of the electronic properties After convergence tests, the structural properties were determined in an iterative process of minimizing the total energy by relaxing the structures and optimizing the lattice parameters and atomic positions.

The results found are in good agreement with the available experimental and theoretical results. The calculations carried out on the electronic structure showed that the three compounds studied are semiconductors. Based on Mulliken's population analysis, and load distribution diagrams.

The analysis of the spectra of the density of electronic states (*PDOS*), allowed us to interpret the spectra of the optical response of the materials studied in a wide range of spectral frequencies. The calculations of the elastic constants showed that our materials are resistive to compression and shear. The elastic constants obtained at 0 *GPa* with the *GGA* obey the mechanical stability conditions of Born, thus indicating the mechanical stability of the monoclinic structure.

The results obtained for the isotropic moduli of elasticity; compressibility modulus B, shear modulus G, and Young's modulus E showed a decrease in values The elastic behavior of these materials indicates that $ABSe_3$ are practically anisotropic, displaying some degree of anisotropy. The B/G ratios show that our materials should be classified as ductile materials.

The results obtained in all parts of this work are consistent and in good agreement with those reported in the literature, which encourages the continuation of this work in the future. this line of research is very interesting, and today, thanks to the scientific and technological impact, the subject is still attracting many researchers around the world. In the end, I hope that the work carried out in this master's thesis will open new perspectives in the ab-initio study of perselenoborate materials.

“If it scares you, it might be a good thing to try.”

Seth Godin

الملخص

في هذا البحث، قمنا بفحص الخصائص الهيكلية، والمرنة، والبصرية، والإلكترونية لمركبات $ABSe_3$ الثلاثية. تشكل هذه المركبات بلورات أحادية الميل، من خلال التعامل مع طاقة التبادل والارتباط من خلال تقريب التدرج المعمم (*PBE*)، استخدمنا نهج حساب ab-initio، وهو نهج إطار دالية الكثافة الإلكترونية (*DFT*) ويتم تنفيذه في رمز *CRYSTAL* ورمز *CASTEP*. باستخدام تقديرات Voigtو Russ وHill قمنا بتقريب معامل الضغط، ومعامل القص، ومعاملYoung، ونسبةPoisson، وغيرها من المعاملات المرنة المتساوية الخواص والخصائص المرتبطة بمراحل البلورة المفردة والبلورات المتعددة باستخدام هذه القيم العددية التي تم الحصول عليها من (C_{ij}s). بما أننا قمنا بفحص الاستقرار الميكانيكي لـ (C_{ij}s) باستخدام البيانات العددية. قمنا أيضًا بتغطية الخصائص البصرية، ومخططات الكثافة الإلكترونية الكلية والجزئية *TDOS* و*PDOS*، والبنيوية، والميزات الإلكترونية الأخرى.

الكلمات الرئيسية : (*DFT*), (CASTEP), Perselenoborates، الخصائص الفيزيائية، المركبات الثلاثية $ABSe_3$

Abstract

In this research, we examined the ternary $ABSe_3$ compounds' structural, elastic, optical, and electrical characteristics. These compounds form monoclinic crystals. By handling the energy of exchange and correlation by the approximation of the generalized gradient *PBE*, we employed the ab-initio calculation approach, which is that of the density functional theory (*DFT*) framework and implemented in the *CRYSTAL* code and *CASTEP* code. Using Voigt, Russ, and Hill approximations, we approximated the bulk modulus, shear modulus, Young's modulus, Poisson's ratio, and other isotropic elastic moduli and associated characteristics for single crystal and polycrystalline phases using these numerical values obtained from the C_{ij}s. Since we checked the mechanical stabilities of C_{ij}s using numerical data. We also briefly covered the optical characteristics, total and partial electronic density diagrams (TDOS and PDOS), band structure, and other electronic features.

Keywords: DFT, CASTEP, Perselenoborates, Physical properties, Ternary compounds $ABSe_3$.

Résumé

Dans cette recherche, nous avons examiné les caractéristiques structurelles, élastiques, optiques et électriques des composés ternaires $ABSe_3$. Ces composés forment des cristaux monocliniques. En traitant l'énergie d'échange et de corrélation par l'approximation du gradient généralisé PBE, nous avons utilisé l'approche de calcul ab-initio, qui est celle du cadre de la théorie de la fonctionnelle de la densité (DFT) et implémentée dans le code *CRYSTAL* et le code *CASTEP*. En utilisant les approximations de Voigt, Russ et Hill, nous avons approximé le module de masse, le module de cisaillement, le module de Young, le coefficient de Poisson et d'autres modules élastiques isotropes et les caractéristiques associées pour les phases monocristallines et polycristallines en utilisant ces valeurs numériques obtenues à partir du C_{ij}s. Depuis, nous avons vérifié les stabilités mécaniques de C_{ij}s à l'aide de données numériques. Nous avons également brièvement couvert les caractéristiques optiques, les diagrammes de densité électronique totale et partielle (TDOS et PDOS), la structure de bande et d'autres caractéristiques électroniques.

Mots clés : DFT, CASTEP, Persélénoborates, Propriétés physiques, Composés ternaires $ABSe_3$